Published in final edited form as:

Dev Cell. 2018 June 18; 45(6): 785–800.e6. doi:10.1016/j.devcel.2018.05.020.

Regulated crossing-over requires inactivation of Yen1/GEN1 resolvase during meiotic prophase I

Meret Arter[1], **Vanesa Hurtado-Nieves**[2,4], **Ashwini Oke**[3,4], **Tangna Zhuge**[3], **Rahel Wettstein**[1], **Jennifer C. Fung**[3], **Miguel G. Blanco**[2,5], and **Joao Matos**[1,5,#]

[1]Institute of Biochemistry, HPM D6.5 - ETH Zürich, Otto-Stern-Weg 3, 8093 Zürich, Switzerland. [2]Departamento de Bioquímica e Bioloxía Molecular, CIMUS, Universidade de Santiago de Compostela - IDIS, 15706 Santiago de Compostela, Spain. [3]Department of Obstetrics, Gynecology, and Reproductive Sciences and Center for Reproductive Sciences, University of California, San Francisco, USA.

SUMMARY

During meiosis, crossover recombination promotes the establishment of physical connections between homologous chromosomes, enabling their bipolar segregation. To ensure that persistent recombination intermediates are disengaged prior to the completion of meiosis, the Yen1(GEN1) resolvase is strictly activated at the onset of anaphase II. Whether controlled activation of Yen1 is important for meiotic crossing-over is unknown. Here, we show that CDK-mediated phosphorylation of Yen1 averts its pervasive recruitment to recombination intermediates during prophase I. Yen1 mutants that are refractory to phosphorylation resolve DNA joint molecules prematurely and form crossovers independently of MutLγ, the central crossover resolvase during meiosis. Despite bypassing the requirement for MutLγ in joint molecule processing and promoting crossover-specific resolution, unrestrained Yen1 impairs the spatial distribution of crossover events, genome wide. Thus, active suppression of Yen1 function - and by inference also of Mus81-Mms4(EME1) and Slx1-Slx4(BTBD12) resolvases - avoids precocious resolution of recombination intermediates to enable meiotic crossover patterning.

eTOC Blurb

[5]Corresponding authors. [#]Lead contact: tel +(41) 44 63 36115, joao.matos@bc.biol.ethz.ch.
[4]Equal contribution

AUTHOR CONTRIBUTIONS

M.A., V.H-N., A.O., T.Z., R.W., J.C.F., M.G.B. and J.M. designed and performed experiments and analyzed data. J.M. conceived the study and wrote the manuscript together with M.A. All authors proofread and contributed to the final manuscript.

SUPPLEMENTAL INFORMATION

Document S1. Figures S1–S7 and Table S1.

DECLARATION OF INTERESTS

The authors declare no competing interests.

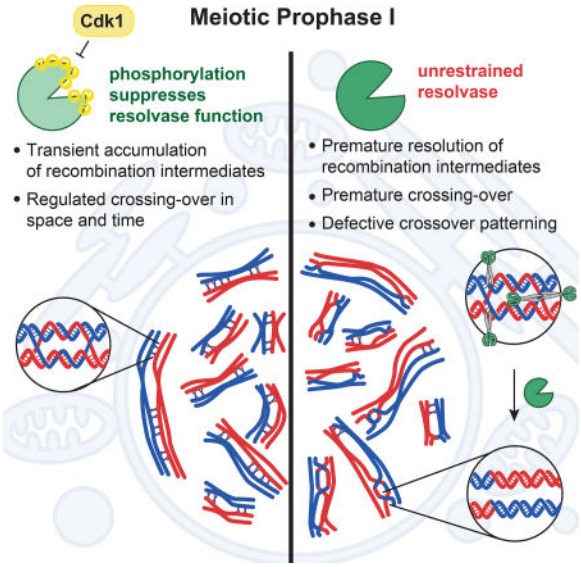

In many organisms, the faithful disjunction of maternal and paternal centromeres during meiosis I requires homologous recombination and crossing-over. Here, Arter et al. show that phosphorylation-mediated inactivation of the Yen1/GEN1 resolvase, during prophase I, avoids the precocious resolution of recombination intermediates to enable controlled crossover formation throughout the genome.

Keywords

Recombination; structure-selective endonuclease; SSE; meiosis; crossover; DNA repair; CDK; cell cycle; Mlh1-Mlh3; Holliday junction

INTRODUCTION

To halve their genome, diploid cells employ a specialized cell division program, meiosis, which consists of one round of DNA replication followed by two consecutive rounds of chromosome segregation: meiosis I and meiosis II. While meiosis II resembles mitosis, the ability of cells to segregate homologous chromosomes during meiosis I entails several specialized events. In most model organisms, physical linkage and subsequent disjunction of maternal and paternal chromosomes require homologous recombination (HR) and crossing-over (Hunter, 2015).

Meiotic HR is initiated by programmed formation of DNA double-strand breaks (DSBs) made by the transesterase Spo11 (Keeney et al., 1997). Upon resection of the broken ends, single stranded 3’-overhangs are generated, which, with the support of recombinases, can invade a homologous DNA sequence for repair (Padmore et al., 1991; Sun et al., 1991). During meiosis, a non-sister DNA duplex is favored as repair template, resulting in the formation of inter-homolog joint molecules (JMs) (Schwacha and Kleckner, 1994, 1995). Differential processing of JMs can then lead to two distinctive outcomes: crossovers (COs), where chromatid arms are reciprocally exchanged; non-crossovers (NCOs), gene conversion

events not associated with reciprocal exchange (Hunter, 2015). Whereas both COs and NCOs contribute to genetic diversity, COs link recombinant chromosomes through sister-chromatid cohesion distal to the exchange site. Therefore, to prevent meiosis I failure and aneuploidy – a prominent cause of miscarriages and birth defects in humans (Hassold and Hunt, 2001) – both the number and the spatial distribution of COs are under stringent control.

In various organisms, including budding yeast, the majority of COs (type I) is non-randomly distributed along chromosomes. Type I COs tend to be widely and evenly spaced by a phenomenon known as “crossover interference” (Zickler and Kleckner, 2016). Spatial patterning of type I COs is thought to involve positive selection and stabilization of a fraction of nascent JMs, in a process termed “crossover designation”. CO designation is supported by ZMM proteins, which stabilize early recombination intermediates and promote their maturation into double Holliday junctions (HJs) (Allers and Lichten, 2001a; Borner et al., 2004; Lynn et al., 2007; Schwacha and Kleckner, 1994; Snowden et al., 2004). CO formation is also temporally controlled. The final nucleolytic resolution of mature JMs into COs is linked to expression of Ndt80, a transcription factor that promotes exit from pachytene (Allers and Lichten, 2001a; Chu and Herskowitz, 1998). Among other M phase regulators, Ndt80 controls the expression of Polo kinase Cdc5, which in turn elicits JM resolution throughout the genome (Clyne et al., 2003; Sourirajan and Lichten, 2008). The vast majority of NCOs – stemming from synthesis-dependent strand annealing – arise before COs and form with normal kinetics in cells lacking *NDT80* or *CDC5* (Allers and Lichten, 2001a; Clyne et al., 2003). Thus, Cdc5 expression triggers JM resolution and CO formation once the majority of NCOs has already formed. If this temporal separation in the formation of NCOs and COs is relevant for meiotic recombination, in particular to the spatial distribution of CO events, has yet to be tested.

At least two separable pathways are involved in the nucleolytic cleavage of mature JMs to generate COs. ZMM-stabilized JMs are resolved as type I COs by the MutLγ nuclease complex (Mlh1-Mlh3) and Exo1 (Argueso et al., 2004; Khazanehdari and Borts, 2000; Ranjha et al., 2014; Rogacheva et al., 2014; Zakharyevich et al., 2010; Zakharyevich et al., 2012). A second class of COs results from the resolution of ZMM-independent JMs by three structure-selective endonucleases (SSEs): Mus81-Mms4(EME1 in humans), Yen1(GEN1) and Slx1-Slx4 (de los Santos et al., 2003; De Muyt et al., 2012; Zakharyevich et al., 2012). SSE-dependent COs do not display spatial interference and are accordingly dubbed ‘type II’ (de los Santos et al., 2003). Despite concurrently resolving meiotic recombination intermediates, MutLγ and SSEs show limited functional overlap: cells lacking MutLγ resolve DNA JMs efficiently, but exhibit lower CO levels and reduced spore viability (Argueso et al., 2004; Wang et al., 1999); conversely, cells lacking *MUS81* and *YEN1* fail to undergo nuclear divisions due to the persistence of unresolved JMs (De Muyt et al., 2012; Matos et al., 2011; Zakharyevich et al., 2012). Although critical to the understanding of how parallel pathways specialize in generating type I and type II COs, the mechanistic basis for the limited resolvase interchangeability is currently missing.

In previous work, we reported that SSEs are tightly regulated by cell cycle stage-specific phosphorylation events in mitotic and meiotic cells. During meiosis, Cdc28(CDK)- and

Cdc5-mediated phosphorylation of Mms4 enhances Mus81-Mms4 nuclease activity at the onset of meiosis I (Matos et al., 2011). As for Yen1, inhibitory phosphorylation restrains its nuclease activity from pre-meiotic S-phase until the onset of meiosis II (Matos et al., 2011). These findings established that coordination of JM resolution with meiotic progression is important to safeguard chromosome segregation. However, they also raised fundamental new questions, including: i) is the active suppression of resolvases necessary for the accumulation of double HJs during prophase I? ii) is this transient accumulation of CO precursors - which covalently link the recombining chromosomes - functionally relevant for meiosis? iii) does SSE regulation prevent pathway competition and explain the limited functional overlap with MutLγ? Moreover, considering that SSEs can target a variety of branched DNA structures in vitro (Dehe and Gaillard, 2017), and given that their regulation is not substrate-specific (Matos et al., 2011), reducing SSE activity during prophase I may be necessary for appropriate JM maturation and breakdown.

We started the present work by asking if controlled SSE activation is broadly required for meiotic recombination. Primed by previous studies that defined the mechanism of Yen1 regulation in mitotic cells (Blanco et al., 2014; Eissler et al., 2014), we have further delineated the mechanism of Yen1 regulation during meiosis. Using a Yen1 mutant refractory to three complementary layers of inhibition we found that active suppression of SSE function, specifically at early stages of meiotic prophase I, is required for the controlled accumulation of ZMM-stabilized JMs and for the correct distribution of COs throughout the genome. This implies that the transient accumulation of recombination intermediates supports the patterning process that positions sites of reciprocal exchange along homologous chromosomes. Analogous regulation of human SSEs may contribute to the fidelity of homolog disjunction during meiosis I, avoiding aneuploidy in gametes.

RESULTS

CDK1-mediated phosphorylation precludes recruitment of active Yen1 nuclease to pachytene chromosomes

In vegetative cells, CDKs regulate Yen1 through a dual mechanism: i) phosphorylation inhibits its nuclease activity by reducing DNA binding; ii) phosphorylation prevents its nuclear accumulation by interfering with nuclear import (Blanco et al., 2014; Eissler et al., 2014). Moreover, mutation of 9 serines in CDK-consensus sites to alanines renders the mutant protein, Yen1^{ON} (Figure 1A), refractory to both layers of regulation. Therefore, to determine if suppression of SSE function is required for appropriate meiotic recombination, we started out by testing if the same set of mutations abolished the regulation of Yen1 in meiotic cells.

To follow the enzymatic activity of Yen1 throughout meiosis, we synchronized yeast cells expressing either Yen1^{WT}-myc9 or Yen1^{ON}-myc9 from the endogenous promoter in G1 (Figure S1A). Following induction of meiosis by transfer to sporulation medium (SPM), samples were collected at 2-hr intervals and Yen1-myc9 was affinity-purified from extracts using anti-Myc beads. HJ resolvase activity was assayed directly by the addition of synthetic Cy3-labeled HJ DNA (see scheme in Figure S1B). In contrast to Yen1^{WT}, which exhibited a sharp increase in activity as cells accumulated meiosis II spindles, Yen1^{ON} displayed potent

resolvase activity during early stages of meiosis, including S phase and prophase I (Figures 1B and 1C). Next, we assessed the subcellular localization of Yen1, which was not previously investigated during meiosis, as a potential second layer of regulation. Immunofluorescence (IF) microscopy showed that $Yen1^{WT}$ is enriched in the nucleus at all stages of meiosis that are characterized by low CDK activity: G1, anaphase I and anaphase II. During S phase, prophase I, metaphase I and metaphase II, $Yen1^{WT}$ was diffuse throughout the cell (Figures 1D and 1E). Consistent with CDK-mediated phosphorylation having an inhibitory role in the nuclear accumulation of Yen1, $Yen1^{ON}$ displayed constitutive nuclear enrichment (Figures 1D and 1E).

To determine if phosphorylation prevents recruitment of Yen1 to recombining chromosomes, we prepared surface spreads from cells expressing myc18-tagged Yen1. Staining of Zip1 and Yen1 revealed that $Yen1^{ON}$, but not $Yen1^{WT}$, formed on average 22 distinct foci per pachytene spread (Figures 1F, 1G and S1C). Consistent with chromatin recruitment being linked to the presence of recombination intermediates, formation of $Yen1^{ON}$ foci was abolished by deletion of *SPO11* (Figures 1F, 1G and S1C). Hence, during meiosis, CDK-mediated phosphorylation inhibits the resolvase activity of Yen1, hinders its active import into the nucleus and precludes its recruitment to recombining chromosomes. $Yen1^{ON}$ is refractory to all three layers of regulation.

Active suppression of Yen1 function prevents untimely resolution of meiotic recombination intermediates

To examine if Yen1 inhibition is required for the appropriate metabolism of meiotic HR intermediates, we performed physical analysis of recombination at the *HIS4-LEU2* hotspot by Southern blot. In brief, digestion of the parental alleles with XhoI produces DNA fragments that are diagnostic for DSBs, JMs and COs. NCOs are detected by conversion of a BamHI/NgoMIV restriction-site polymorphism at the DSB formation site (Hunter and Kleckner, 2001; Kim et al., 2010; Schwacha and Kleckner, 1995).

In control cells expressing Yen1 ($YEN1^{WT}$), formation of DSBs followed DNA replication and peaked ~5 hrs after the induction of meiosis. JMs reached a maximum at ~7 hrs and COs plateaued after 10 hrs in SPM (Figure 2A and 2B, S2A–D). $YEN1^{ON}$ mutants formed DSBs with comparable kinetics to control cells but displayed a marked reduction in the accumulation of JMs (Figures 2A–B). Nevertheless, $YEN1^{ON}$ cells still generated COs and NCOs to similar levels and with comparable kinetics to controls cells (Figure S2B–D).

Since the final level of COs and NCOs in $YEN1^{ON}$ mutants was similar to that of control cells, we hypothesized that the reduced accumulation of JMs could derive from premature, Ndt80-independent resolution of CO-precursors (i.e. ZMM-stabilized JMs or earlier intermediates). Such model would imply that COs form prematurely in $YEN1^{ON}$ cells, which we failed to observe (Figure S2D). However, since the synchrony of meiotic cultures is limited, small differences - ~30 min (Allers and Lichten, 2001a) - in the timing of CO formation, relative to NCOs, may be difficult to detect. Therefore, we analyzed *ndt80Δ* mutants, which accumulate JMs and display a concurrent defect in the formation of COs (Allers and Lichten, 2001a; Sourirajan and Lichten, 2008). Despite undergoing efficient DNA replication and forming seemingly normal levels of DSBs, *ndt80Δ* $YEN1^{ON}$ cells

showed a prominent defect in JM accumulation (Figure 2C–D, S2E). Analysis of the recombination outcome revealed a significant increase in the formation of COs, which occurred alongside a decrease in NCOs (Figure 2D, S2F–G). Combined, this led to an increase in the CO/NCO ratio from 0.2 to 1.2 (Figure 2E), which was similar to the CO/NCO ratio of *NDT80* cells (Figure S2C–D).

Next, we asked if JM resolution and premature CO formation triggered by Yen1^{ON} was dependent on MutLγ. Analysis of recombination at *HIS4-LEU2* revealed that *ndt80Δ mlh3Δ YEN1^{ON}* mutants accumulate less JMs than control *ndt80Δ mlh3Δ YEN1^{WT}* cells (Figure 2F–G, Figure S2H). Together with the reduction in JM accumulation, cells carrying *YEN1^{ON}* again showed a marked increase in the formation of COs, altering the CO/NCO ratio from 0.2 to 1.1 (Figure 2F–H and S2H–J).

In summary, these data indicate that CDK-mediated phosphorylation of Yen1 is required for the transient accumulation of ZMM-stabilized JMs, without unequivocally distinguishing if it directly targets mature JMs, nascent JMs or a mixture of the two. Irrespective of the substrate(s) cleaved, the above data demonstrate that active suppression of Yen1 function is necessary for the coupling of CO formation to exit from pachytene.

Unrestrained Yen1 function improves crossover formation, chromosome segregation and spore viability in cells lacking MutLγ, Mus81-Mms4 and Sgs1

To complement the physical analyses of recombination, we used spore autonomous fluorescent markers (Thacker et al., 2011) to determine if unrestrained Yen1 was sufficient to restore CO formation at the *CEN8-THR1* interval in cells lacking MutLγ-Exo1 (Figure 3A, S3A). As expected in a *YEN1^{WT}* background, deletion of *MLH1, MLH3* or *EXO1* led to a significant reduction in genetic distance, from 18.6 ± 0.5 (*WT*) to 10.0 ± 0.4 (*mlh1Δ*), 9.2 ± 0.4 (*mlh3Δ*) and 8.9 ± 0.4 (*exo1Δ*) cM (Argueso et al., 2004; Khazanehdari and Borts, 2000). In cells carrying *YEN1^{ON}*, the measured genetic distance was largely independent of MutLγ-Exo1: 18.1 ± 0.8 (*WT*), 20.1 ± 0.6 (*mlh1Δ*), 17.4 ± 0.6 (*mlh3Δ*) and *15.6* ± 0.7 (*exo1Δ*) cM (Figure 3B, S3B). It is well established that defective CO formation leads to homolog non-disjunction. In line with the observed increase in genetic distance (Figure 3B), the *YEN1^{ON}* allele restored segregation of chromosome VIII in all mutant backgrounds (Figure 3C, S3B). These data suggest that inhibition of Yen1 prevents MutLγ-independent formation of COs at *CEN8-THR1*.

Since *HIS4-LEU2* and *CEN8-THR1* may not accurately represent other chromosomal regions, we queried if Yen1^{ON} was sufficient to broadly suppress the chromosome segregation and spore viability defects associated with loss of MutLγ-Exo1 and Mus81 (De Muyt et al., 2012; Matos et al., 2011; Zakharyevich et al., 2012). To directly visualize chromosome segregation, we generated strains in which both homologs of chromosome V were marked by GFP at *URA3* (homozygous *URA3-GFP*) and a myc18-tagged version of the anaphase inhibitor Pds1 was expressed (Salah and Nasmyth, 2000). In a *YEN1^{WT}* background, *mus81Δ* and *mlh3Δ* mutants presented two distinctive phenotypes in anaphase I (cells with a bipolar spindle and no Pds1): 1) 83.5% of *mus81Δ* cells failed to undergo nuclear division as measured by detection of a single DNA mass; 2) *mlh3Δ* mutants displayed a relatively normal nuclear division but frequently missegregated chromosome V

(10% non-disjunction). In a *YEN1*^{ON} background, both defects were significantly reduced: 74% of *mus81Δ* cells underwent complete nuclear division and 99% of *mlh3Δ* cells segregated chromosome V efficiently (Figures 3D–F, S3C–D).

To further test the ability of unrestrained Yen1 to resolve recombination intermediates, we generated *mus81Δ mlh3Δ sgs1-mn* (meiotic-null) triple mutants. Due to the lack of all key pathways of JM processing that operate during meiosis I, such triple mutants accumulate lethal levels of JMs (De Muyt et al., 2012; Zakharyevich et al., 2012). In the presence of Y*EN1*^{WT}, 54.5% of the cells failed to disjoin chromosome V and 97.5% failed to undergo nuclear division at anaphase I (Figure 3D–F). In a *YEN1*^{ON} background, chromosome V was segregated efficiently in 90.5% of the cells and 48% of anaphases were accompanied by a complete nuclear division (Figure 3D–F, S3C–D).

Since defective JM processing generally leads to formation of aneuploid spores, we also assessed spore viability. Notably, *YEN1*^{ON} significantly improved spore survival in all mutant backgrounds analyzed, including *mus81Δ mlh3Δ sgs1-mn* triple mutants (Figures 3G–H, S3E). This indicates that Yen1 function during early stages of meiosis is sufficient to resolve most DNA JMs, independently of the chromosomal region. It is also interesting to note that the increase in spore viability of *mlh1Δ* and *sgs1Δ* single mutants was only moderate, which may reflect their additional – pre-meiotic or meiotic – roles in mismatch repair and in the metabolism of nascent JMs, respectively (Duroc et al., 2017; Hunter and Borts, 1997; Jessop and Lichten, 2008; Oh et al., 2007).

In summary, Yen1 activity during prophase I is sufficient to restore JM resolution (genome-wide) and CO formation (at the *HIS4-LEU2* and *CEN8-THR1* intervals), as well as chromosome segregation and spore viability to mutants defective in processing late recombination intermediates. This supports the notion that Yen1 inhibition prevents widespread resolution of HR intermediates throughout the genome.

Unrestrained Yen1 function is deleterious to spore viability

While analyzing the consequences of Yen1^{ON} expression to spore viability in different mutant backgrounds, we noticed that the observed improvements were never complete. In most mutant backgrounds spore viability was capped at approximately 80–90% (Figure 3G, S3E). Therefore, we suspected that while having an overall beneficial effect in mutants with defective JM processing, Yen1^{ON} might be deleterious to meiosis. In agreement with this possibility, *YEN1*^{ON} strains displayed lower spore viability, ~90% of the control *YEN1*^{WT} (Figure 4A). Despite being modest, this reduction in viability is comparable to the one caused by full loss of *MLH3* (~85% of the wild type levels) (Figure 3G). To determine if the observed phenotypes depended on recombination, we analyzed spore viability in *spo11Δ mam1Δ* double mutants, which form viable dyads upon segregation of sister chromatids in a single meiotic division (Toth et al., 2000) (Figure 4B, left scheme). In this background, *YEN1*^{ON} did not cause spore lethality (Figure 4B, right panel). Hence, while able to improve the resolution of DNA JMs in several mutant strains, unrestrained Yen1 function is overall detrimental to meiosis most likely due to its effect on recombination.

Unrestrained Yen1 activity impairs the spatial distribution of COs

ZMM proteins and MutLγ-Exo1 are required for the formation of class I COs, which show spatial interference (Borner et al., 2004; De Muyt et al., 2012; Hunter, 2015; Mancera et al., 2008; Zakharyevich et al., 2012). Since Yen1^{ON} improved CO formation in cells lacking MutLγ-Exo1 or ZMMs (Figure 2F–H, 3B, data not shown), we asked if CO interference was similarly restored. To this end, we used the three-marker system (Figure 3A) and queried if a CO event in the first interval (*CEN8-ARG4*) affected the probability of occurrence of another CO in the second interval (*ARG4-THR1*). Despite the robust rescue in CO formation, *YEN1^{ON}* did not improve CO interference, as measured genetically, in any of the mutants analyzed (Figure 4C). Moreover, in an otherwise wild type background, *YEN1^{ON}* reproducibly led to an increase in the frequency of co-occurring COs in the adjacent intervals. A similar effect of *YEN1^{ON}* was observed in *mus81Δ* mutants, which are specifically defective in forming type II COs (de los Santos et al., 2003) (Figure 4C). Thus, control of JM resolution during prophase I is necessary for the appropriate spacing of COs at *CEN8-THR1*.

To further scrutinize these findings genome-wide, we turned to next-generation sequencing of single nucleotide polymorphisms in haploid spores generated from hybrid yeast strains (Figures 4D and S4A) (Chen et al., 2008; Mancera et al., 2008). In agreement with the *CEN8-THR1* hotspot data, expression of Yen1^{ON} from the endogenous promoter led to a significant defect in the spatial distribution of COs, as revealed by the gamma distribution of inter-JM distances (γ=1.45 in *YEN1^{ON}* and γ=1.95 in wild type). This defect occurred in the absence of a significant change to the overall number of COs, NCOs, or to the CO/NCO ratio (Figures 4E–F, S4B–C). Given that the observed defect in CO distribution was only partial, we asked if MutLγ and ZMMs contributed to the remaining patterning of CO events. Indeed, despite presenting increased CO levels, *mlh3Δ YEN1^{ON}* and *msh4Δ YEN1^{ON}* double mutants showed a stronger defect in the gamma distribution of inter-CO distances (γ=1.18 and γ=1.1, respectively) (Figures 4G–H). Interestingly, *mlh3Δ YEN1^{WT}* cells displayed an intermediate defect in the gamma distribution (γ=1.39), suggesting that *YEN1^{ON}* impairs CO patterning by a mechanism that is in part distinct from the one caused by loss of MutLγ (Figure S4D–E). Overall, our data confirm that Yen1 inhibition during prophase I is required for the regular distribution of CO events, genome-wide. In cells with uncontrolled Yen1 function, ZMMs and MutLγ are only partly capable of implementing the formation of spatially patterned COs.

To explain the findings described above one could envisage that, in contrast to MutLγ, Yen1^{ON} resolves correctly designated and interfering JMs as a mixture of COs and NCOs. This possibility would be consistent with the slight reduction in COs and increase in NCOs which we detect in *mlh3Δ YEN1^{ON}*, relative to *YEN1^{ON}* (Figure 4H). However, this model would also predict that – in an otherwise wild type background – *YEN1^{ON}* should cause a specific reduction in the overall frequency of COs and in the CO/NCO ratio, which we consistently failed to detect (Figure S2D, 3B and S4C). A second possibility is that correct designation of JMs is disrupted in the presence of Yen1^{ON}. For example, Yen1^{ON} could prematurely resolve a fraction of nascent JMs, producing COs without prior designation, as proposed for fission yeast Mus81-Eme1 (Lorenz et al., 2012; Osman et al., 2003). As a

variant of this possibility, Ndt80-independent resolution of CO-designated JMs by Yen1^{ON} may prevent interference between JMs, if only JMs but not COs can inhibit designation of nearby recombination intermediates to become COs.

Phosphorylation-resistant Yen1 nuclease resolves ZMM-stabilized JMs during pachytene

To discriminate between the models outlined above, it is important to understand if Yen1^{ON} is capable of resolving mature JMs containing double HJs or if it prevents JM accumulation by processing precursor intermediates (Allers and Lichten, 2001b; Hunter and Kleckner, 2001). In vitro, besides cleaving single and double HJs efficiently, Yen1 and GEN1 also cleave nicked HJs and displacement loop structures (Blanco et al., 2014; Matos et al., 2011; Shah Punatar et al., 2017)(V. Hurtado-Nieves and M. G. Blanco, unpublished observations). Hence, to determine if Yen1 can directly target ZMM-stabilized HR intermediates containing double HJs, we let *ndt80Δ* strains accumulate in pachytene, at which point JMs have matured to contain such structures (Allers and Lichten, 2001a; Sourirajan and Lichten, 2008). After most cells reached pachytene, as monitored by staining of the synaptonemal complex (Figure 5A–B), we initiated expression of Yen1^{ON}-FLAG. For that purpose, we used a Gal4-estrogen receptor fusion to induce the *GAL1* promoter with β-estradiol (Benjamin et al., 2003). Notably, induction of Yen1^{ON} expression caused a marked reduction in the levels of JMs and a concurrent increase in the formation of COs (Figure 5C–D). By contrast, cells expressing inducible Yen1^{WT} kept gradually accumulating JMs and formed comparably fewer COs (Figure 5C–D).

To verify if JM resolution triggered by Yen1^{ON} was dependent on its nuclease activity, we engineered strains conditionally expressing Yen1$^{ON\text{-}ND}$, which contains two additional mutations in the nuclease active site, E193A and E195A (Blanco et al., 2014). Yen1$^{ON\text{-}ND}$ expression did not alter JM accumulation or CO formation, which were comparable to control cultures treated with MeOH (Figure 5E–F, S5). We conclude that phosphorylation-resistant Yen1 resolves ZMM-stabilized JMs efficiently.

CO-specific resolution of ZMM-stabilized JMs by Yen1

SSEs are thought to resolve individual HJs within double HJs in an uncoordinated manner, thus generating COs and NCOs at random (West et al., 2015). This notion is supported by in vivo work in mitotic cells (Dayani et al., 2011) and by in vitro resolution of synthetic double HJs (Shah Punatar et al., 2017). By contrast, physical analysis of recombination in meiotic cells established that MutLγ-Exo1 promotes the resolution of ZMM-stabilized JMs to generate COs, exclusively (Zakharyevich et al., 2012). Whether MutLγ-Exo1 is unique in its ability to promote CO-specific resolution of double HJs is unknown. As described above, induction of Yen1^{ON} expression is sufficient to drive the resolution of mature JMs, in *ndt80Δ* cells. Thus, we examined if JM resolution yielded COs, or a mixture of COs and NCOs. Yen1^{ON} expression in cells treated with β-estradiol was sufficient to trigger JM resolution, while control cultures treated with MeOH accumulated JMs over time, as expected (Figure 6A and S6A). Importantly, however, while we detected a robust increase in the formation of COs that was specific to cells expressing Yen1^{ON}, NCOs formed with comparable kinetics and to similar levels in both conditions (Figure 6B–C).

Since Yen1^{ON} expression triggered CO-specific JM resolution, we asked if the CO bias was dependent on MutLγ-Exo1. Physical analysis of recombination showed that neither the overall efficiency of JM resolution, nor the specific formation of COs, was altered in *mlh1Δ* and *mlh3Δ* mutants (Figure 6D–F, S6B). Moreover, similar results were obtained with cells expressing a "nuclease-dead" version of Mlh3, Mlh3-ND (Nishant et al., 2008) (Figure 6D–E, S6B). In all cases, expression of Yen1 significantly increased the CO/NCO ratio (Figure 6G). Thus, we conclude that unrestrained Yen1 is capable of promoting efficient and CO-specific resolution of ZMM-stabilized JMs, independently of MutLγ. This suggests that CO-designated double HJs may adopt specialized configurations, or marks, that favor the coordinated cleavage of the crossing and non-crossing strands in the individual HJs to ensure CO-specific resolution.

Pachytene-specific expression of Yen1^{ON} triggers premature JM resolution without disrupting the spatial distribution of COs

Since Yen1 was capable of triggering CO-specific resolution of mature JMs, we suspected that the defective spatial distribution of CO events observed in *YEN1^{ON}* mutants (Figure 4C and E) does not result from the aberrant resolution of CO-designated JMs to generate COs and NCOs. We rather focused on the possibility that it might be linked to the asynchronous, Ndt80-independent, processing of CO precursors. One prediction of this model would be that expression of Yen1^{ON} after arrest in pachytene, as in Figure 5C, would not impact CO interference. To test this prediction, we generated *ndt80Δ* strains combining the three-marker spore-fluorescence system (Figure 3A) with inducible Yen1^{ON} (P$_{CUP1}$-*YEN1^{ON}*) and inducible Ndt80 (P$_{GAL1}$-NDT80). We then released cells to synchronously enter meiosis and initiated Yen1^{ON} expression after the completion of DNA replication (5 hrs in SPM) or after JM accumulation in pachytene (7 hrs in SPM) (Figure 7A). Ndt80 expression was then induced in both cultures 9 hrs after transfer to SPM, allowing cells to complete meiosis (Figure 7A). In contrast to early expression of Yen1^{ON}, which impaired CO interference, late expression of Yen1^{ON} did not visibly affect the frequency of concurrent COs at *CEN8-ARG4* and *ARG4-THR1* (Figure 7B–D and Figure S7A–B). These data further support the notion that transient accumulation of mature and/or maturing JMs is necessary for the appropriate spatial distribution of reciprocal exchanges between homologous chromosomes.

DISCUSSION

We started the present work by investigating the mechanism of Yen1 regulation during meiosis. In a first step, we found that Yen1 function is inhibited by CDK-mediated phosphorylation during meiotic prophase I – precisely when JMs arise (Figure 7E). Phosphorylation impacts nuclease activity, nuclear import and chromatin recruitment of Yen1. In support of these findings, we showed that Yen1^{ON}, a mutant refractory to CDK-mediated phosphorylation (Blanco et al., 2014; Eissler et al., 2014), is constitutively active, nuclear and precociously recruited to recombining chromosomes. Having such a unique tool in hand has allowed us to: i) elucidate the functional significance of Yen1/SSE regulation during meiosis; ii) learn about the mechanism of CO-specific JM resolution; iii) study the interplay between the temporal and spatial control of crossing-over.

Active suppression of SSE function is required for the accumulation of ZMM-stabilized joint molecules and supports spatial crossover patterning

Previous work revealed that Yen1 nuclease is strictly activated at the onset of the second meiotic division to safeguard the resolution of persistent recombination intermediates (Matos et al., 2011) (Figure 7E). We now show that controlled activation of Yen1 is required to avoid untimely resolution of DNA JMs throughout the genome. As a consequence of premature JM processing, cells with unrestrained Yen1 generate COs prematurely, which as a result are inappropriately spaced (Figure 7E and S7C–D). Overall, unrestrained Yen1 function also impairs spore viability, demonstrating that SSE control is of general relevance for meiosis.

Local chromosomal context has been proposed to influence the choice of proteins that resolve recombination intermediates to form COs (Medhi et al., 2016). Our work now suggests that unrestrained Yen1 nuclease resolves HR intermediates, including ZMM-stabilized JMs, throughout the genome. This implies that CO designation and local chromosomal context are not sufficient to prevent pathway competition and ensure CO implementation by MutLγ-Exo1. Hence, we propose that pathway usage is established through the combination of at least two modes of resolvase regulation that act in the following sequence: 1) temporal suppression of SSEs clears the way for MutLγ-Exo1 function during prophase I; 2) chromosomal context spatially confines MutLγ recruitment to a subset of CO-designated recombination intermediates. This dual mode of regulation ensures that MutLγ function is restricted to promoting CO formation at tightly patterned sites of recombination. In turn, SSEs safeguard that all JMs that are not channeled towards MutLγ are processed in time for chromosome segregation.

Meiosis-specific properties of DNA joint molecules support crossover-specific resolution

It has been proposed that MutLγ is uniquely able to promote biased JM resolution to generate exclusively COs (Zakharyevich et al., 2012). Our work now shows that – provided that it is active during meiotic prophase I – Yen1 can also resolve JMs to generate COs. This surprising finding implies that biased JM processing does not necessarily depend on the resolvase used, but rather on specific properties of the chromosomal substrate, such as whether or not Zip3 is associated with the JM (Oke et al., 2014). This may help explain how some organisms, including *S. pombe, C. elegans* and *D. melanogaster* utilize SSEs as the main source of COs (Agostinho et al., 2013; O'Neil et al., 2013; Osman et al., 2003; Saito et al., 2013; Smith et al., 2003; Yildiz et al., 2002). If biased JM resolution is rather dependent on substrate presentation, any variation in pathway usage will be compatible with the highly conserved need to assure the formation of at least one CO per homolog pair. One prediction of this model is that SSE regulation may be different in different organisms. In those that do not depend on MutLγ for CO formation, a special emphasis on the spatial regulation of SSE function – reminiscent of MutLγ control – may be needed. It is however important to note that our results do not exclude that specialized properties of MutLγ may contribute to biased JM processing, neither do they imply that Yen1 and MutLγ resolve recombination intermediates using the same mechanism. Recent in vitro work suggests that, in contrast to SSEs, MutLγ may not cleave double HJs (Manhart et al., 2017). Future studies will be required to further clarify the precise in vivo substrate of MutLγ and to identify factors

required for biased JM processing. By combining the inducible expression of Yen1^{ON} (Figure 6D) with mutation of candidate genes, we anticipate it will now be feasible to directly screen for factors necessary for CO-specific resolution.

Is the accumulation of JMs - potential barriers to chromosome segregation - and their concerted resolution at the onset of metaphase I functionally relevant for meiosis?

One of the most fascinating aspects of meiosis is the process that establishes the position of COs along chromosomes. It was noted more than a century ago that COs are spatially regulated (Muller, 1916) but the mechanistic basis of such distribution remains a matter of intense research (Zickler and Kleckner, 2016). More recent findings demonstrate that CO formation is also temporally regulated. ZMM-stabilized JMs pile up during prophase I, only to be resolved as cells prepare to segregate maternal and paternal homologs during meiosis I (Figure 7E) (Allers and Lichten, 2001a, b; Hunter and Kleckner, 2001; Schwacha and Kleckner, 1995). Whether the appropriate spatial patterning of CO events is linked to the transient accumulation of recombination intermediates was unknown. By repurposing Yen1 to induce JM resolution at different times after their formation, we were able to show that conditions that prevent JM accumulation are disruptive to CO distribution, while premature JM processing in cells pre-synchronized in pachytene is not. Thus, we suggest that transient accumulation of DNA JMs is indeed important for appropriate CO patterning.

We hypothesize that untimely resolution of a JM (CO-designated or non-designated) into a CO might allow for inappropriate stabilization and designation of a nascent JM in the vicinity (Figure S7D). This model is consistent with previous studies that described non-random spatial distribution of the ZMM proteins Zip2 and Zip3, which are likely to mark early CO precursors (Fung et al., 2004; Zhang et al., 2014). In essence, this would suggest that meiotic cells restrain the function of SSEs, and amass dozens of mature JMs along chromosomes, in order to allow for “safe” processing of non-designated JMs into NCOs (Figure 7E and S7C). Once DSB repair has finished and non-designated JMs have been converted to NCOs, the recombination checkpoint licenses Ndt80-dependent exit from pachytene (Tung et al., 2000), which temporally coordinates CO-specific JM resolution. A potential implication of this working model is that once a CO has formed, there is no mechanism in place to discourage the formation of a CO in the vicinity. Hence, despite not being involved in the patterning process *per se*, regulation of both MutLγ and SSEs is important in ensuring appropriate CO distribution. This is particularly interesting in light of recent findings demonstrating that inappropriate CO configurations and age-dependent alterations in resolvase usage lead to chromosome segregation errors and aneuploidy in gametes (Wang et al., 2017; Zelazowski et al., 2017).

STAR METHODS

Contact for Reagent and Resource Sharing

Further information and requests for resources and reagents should be directed to and will be fulfilled by the Lead Contact, Joao Matos (joao.matos@bc.biol.ethz.ch).

Experimental Model and Subject Details

All strains were SK1, YJM789 or S96 derivatives, as detailed in Table S1. The following alleles have been described previously: *mam1Δ, ndt80Δ, spo11Δ, PDS1-myc18, mus81Δ,* P_{GPD1}*-GAL4-ER*, spore-autonomous fluorescent markers for the live-cell recombination assays, as well as the *HIS4-LEU2* alleles for physical analysis of recombination (Kim et al., 2010; Matos et al., 2011; Petronczki et al., 2006; Thacker et al., 2011). The *CLB2* promoter was used for meiosis-specific depletion of Sgs1 (Lee and Amon, 2003). Strains containing *URA3* marked with GFP and P_{GAL1}*-NDT80* were kindly provided by Wolfgang Zachariae (MPI, Munich). Strains carrying β-estradiol-inducible $YEN1^{WT}$ and $YEN1^{ON}$ (P_{GAL1}-$YEN1^{WT}$*-FTH,* P_{GAL1}-$YEN1^{ON}$*-FTH*) were generated by inserting the *YEN1-FTH* (*FLAG3-TEV2-HIS10*) sequences into the pAG304GAL-ccdB destination vector using Gateway cloning and integrating the construct at the *TRP1* locus. Strains carrying copper-inducible $YEN1^{ON}$ (P_{CUP1}-$YEN1^{ON}$*-Myc9*) were generated by one-step promoter replacement in a strain carrying *YEN1-Myc9*. Strains carrying $YEN1^{ON}$ at the endogenous locus were generated using *delitto perfetto* (Storici and Resnick, 2003) or by backcrossing of strain W1458 (Blanco et al., 2014) to SK1 (>6 times). $YEN1^{ON\text{-}ND}$ is a Nuclease-Dead version of $YEN1^{ON}$ by encoding the following mutations: E193A and E195A (Blanco et al., 2014). $MLH3^{ND}$ is a Nuclease-Dead version of *MLH3* by encoding the following mutation: D523N (Nishant et al., 2008).

For C-terminal PCR-based tagging of chromosomal genes with the Myc9 and Myc18 epitopes, cassettes were amplified from plasmids as described (Knop et al., 1999). Gene deletions were introduced into SK1 by PCR-based amplification of cassettes from the yeast knock-out collection.

Method Details

Meiotic time courses—Meiotic time courses were performed as described (Petronczki et al., 2006). Briefly, colonies grown on YP-glycerol plates (2% peptone, 1% yeast extract, 2% glycerol, 2% agar) for 48 hrs at 30°C were transferred and spread on YPD plates (2% peptone, 1% yeast extract, 2% dextrose, 2% agar) and grown to form a small lawn (~24 h, 30°C). Cells were then transferred to YPD plates and grown into a lawn (~24h, 30°C), which was then used to inoculate pre-sporulation medium $YP_{2\%KAc}$ (2% peptone, 1% yeast extract, 2% KAc) to OD_{600} ~0.3. Cells were grown for either 14 hr (25°C) or 11 hr (30°C), washed with sporulation medium (SPM, 2% KAc) and inoculated into SPM to OD_{600} ~3.5. This time point was defined as t = 0 in all meiotic experiments. Induction of Yen1 expression in prophase I-arrested cells (P_{GAL1}-$YEN1^{WT}$*-FTH or* P_{GAL1}-$YEN1^{ON}$*-FTH* was initiated by addition of 1 μM β-estradiol. Induction of $Yen1^{ON}$ expression from the copper-inducible promoter was initiated by addition of 1 μM $CuSO_4$. Cellular DNA content was determined using a FACSCalibur cytometer (Becton Dickinson) running CellQuest software.

Fluorescence microscopy—Yeast cells were processed for immunostaining as described (Matos et al., 2011). Briefly, cells were fixed with 3.7% formaldehyde overnight and treated with Zymolase 100T. Spheroplasts were seeded on microscopy slides coated with Poly-L-lysine and stained using the following antibodies: mouse monoclonal anti-Myc 9E10 (1:100), rat anti-tubulin (1:600), rabbit anti-Myc (1:500), rabbit anti-Zip1 (1:100),

rabbit anti-GFP (1:500). Secondary antibodies conjugated to Alexa555, Alexa488 and Alexa647 were used for detection (1:300). DNA was stained with 4',6-diamidino-2-phenylindole (DAPI). Images were acquired using a DeltaVision personalDV multiplexed with a 60× 1.4NA DIC Oil PlanApoN objective and a Roper CoolSnap HQ2 camera under the control of Softworx Version 4.1.0 (Applied Precision) software. Images were processed using Fiji.

Yeast protein analyses—Protein analysis in yeast was performed as described previously (Matos et al., 2008). Briefly, meiotic cultures (OD_{600} ~3.5, 10 ml) were disrupted using glass beads in 10% TCA. Precipitates were collected by centrifugation, resuspended in 2× NuPAGE sample buffer, and neutralized with 1 M Tris. Samples were boiled at 95°C for 5 min, cleared by centrifugation, and separated in NuPAGE 4–12% Bis-Tris or NuPAGE 3–8% Tris-Acetate gels (Invitrogen). Gels were blotted on PVDF membranes (GE Healthcare).

Immunoprecipitates were prepared from 50–100 ml of meiotic culture. Cells were lysed with glass beads in buffer R (40 mM Tris, pH 7.5, 150 mM NaCl, 10% glycerol, 0.1% NP40) containing protease and phosphatase inhibitors. Protein extracts were cleared and normalized (7.5 mg protein in 700 µl) and epitope-tagged proteins were captured using mouse monoclonal antibodies to Myc (9E10) coupled to agarose beads (AminoLink Plus). For immunoblotting, we used antibodies to the following proteins or epitope tags: Myc HRP-conjugated (1:25000), FLAG HRP-conjugated (1:5000), Puf6 (1:5000), Cdc5 (1:200), Pgk1 (1:10000).

Nuclease assays—For nuclease assays, myc9-tagged Yen1 was immuno-affinity purified from yeast using anti-Myc agarose beads (9E10) and washed extensively. The beads (approx volume 10 µl) were then mixed with 10 µl cleavage buffer (50 mM Tris-HCl pH 7.5, 3 mM $MgCl_2$) and 15 ng of 5'-Cy3-end-labeled synthetic Holliday junction X0 DNA (Ip et al., 2008). After 1 h incubation at 37°C with gentle rotation, reactions were stopped b y addition of 2.5 µl of 10 mg/ml proteinase K and 2% SDS, followed by incubation for 30 min at 37°C. Loading buffer (3 µl) was then added and fluorescently-labeled products were separated by 10% native PAGE and analysed using a Typhoon scanner and ImageQuant software. Resolution activity was calculated by determining the fraction of nicked duplex DNA product relative to the sum of the intact substrate and resolution product. The protein input was estimated by western blot.

Analysis of recombination using spore-autonomous fluorescence—The spore-autonomous fluorescence recombination analysis was performed as described previously (Thacker et al., 2011). After synchronization, diploid yeast cells were inoculated into SPM to OD600 ~3.5 and incubated at 30°C. After 48–60 hrs, images were captured in four channels using a DeltaVision personalDV multiplexed with a 60× 1.4NA DIC Oil PlanApoN objective and Roper CoolSnap HQ2 camera under the control of Softworx Version 4.1.0 (Applied Precision) or a Leica DM 6000B microscope using a HCX PL Fluotar 63×, oil objective lens, and captured using an ORCA C4742-95-12ER camera (Hamamatsu) controlled by Openlab 5.0.2 software (Improvision). The pattern of fluorescence in the tetrads was manually scored using Fiji. Only tetrads with four spores and each fluorescence marker occurring in two spores were included in the final analysis. Recombination

frequency, expressed as map distance in centimorgans with standard error, was calculated using the Stahl lab online tools. Crossover interference ratio was calculated as described (Thacker et al., 2011). For every strain, > 430 tetrads were scored based on at least two independent experiments.

Genome-wide analysis of recombination—DNA was prepared for Illumina sequencing using a NextFlex kit (BIOO) with Illumina-compatible indices or as described (Anderson et al., 2011) with 4-base or 8-base inline barcodes. Read alignment, genotyping and recombination mapping were performed using the ReCombine package (Anderson et al., 2011). While running CrossOver.py, the input values for 'closeCOs', 'closeNcoSame' and 'closeNCODiff' were all set to 0. Insertions and deletions were removed from the set of genotyped markers. Recombination events within 5kb of each other were then merged into single events and categorized into seven types as described (Oke et al., 2014). Gamma distributions and CoC were calculated as described (Anderson et al., 2015).

Physical analysis of recombination at the *HIS4-LEU2* locus—DNA physical assays were performed as described before (Kim et al., 2010; Matos et al., 2011). In brief, cells from 50–100 mL cultures were treated with psoralen. Crosslinking was induced using a SpectroLinker XL-1500 crosslinker (Spectroline). The crosslinking time was 5–10 min during which the cells were kept on ice and mixed at regular intervals. After DNA extraction genomic DNA concentrations were quantified using the Qubit dsDNA broad range kit. Restriction enzyme-digested DNA (~2 μg) was separated by electrophoresis on 0.6% agarose gels. Recombination intermediates were quantified by phosphorimaging using a Typhoon scanner. Different recombination intermediates were quantified by determining the signal of each species relative to the total lane signal using ImageQuant software. Background subtraction was done manually by subtracting the signal at time point 0 from all measurements.

Analysis of spore viability and other quantifications—Spore viability was determined by microdissection of > 432 spores from 6 biological replicates. Standard errors were calculated using Excel. The quantitative analyses of cell cycle stage progression (spindle morphology and nuclear division) and pattern of chromosome segregation were performed by the examination of >200 cells for each variable.

Quantification and Statistical Analysis—All statistical analyses were compiled using Prism software and Microsoft Excel. For multiple comparisons, analysis of variance (one-way ANOVA) was performed with Prism, followed by Tukey’s multiple comparison test. For pairwise comparisons two-tailed, unpaired t-tests were used.

Data and Software Availability—Raw sequence data from the genome-wide analysis of recombination have been deposited in the NIH Sequence Read Archive under accession number SRP144029.

Supplementary Material

Refer to Web version on PubMed Central for supplementary material.

Acknowledgments

We thank Scott Keeney, Nancy Kleckner and Wolfgang Zachariae for strains and plasmids; Jérôme Zürcher for help with tetrad dissections. Attila Toth, Joe Jiricny and Rokas Grigaitis for critical reading of the manuscript. ScopeM at ETH Zürich provided the imaging facility. The Blanco lab is supported by MINECO, AEI, Xunta de Galicia and FEDER (RYC-2012-10835, BFU2013-41554-P, BFU2016-78121-P, ED431F-2016/019, ED431B-2016/016 and BES-2014-068734). The Fung lab is supported by NIH R01 GM116895. The Matos lab is supported by ETH Zürich and the Swiss National Science Foundation (31003A_153058 and 155823).

References

Agostinho A, Meier B, Sonneville R, Jagut M, Woglar A, Blow J, Jantsch V, Gartner A. Combinatorial regulation of meiotic holliday junction resolution in C. elegans by HIM-6 (BLM) helicase, SLX-4, and the SLX-1, MUS-81 and XPF-1 nucleases. PLoS Genet. 2013; 9:e1003591. [PubMed: 23901331]

Allers T, Lichten M. Differential timing and control of noncrossover and crossover recombination during meiosis. Cell. 2001a; 106:47–57. [PubMed: 11461701]

Allers T, Lichten M. Intermediates of yeast meiotic recombination contain heteroduplex DNA. Mol Cell. 2001b; 8:225–231. [PubMed: 11511375]

Anderson CM, Chen SY, Dimon MT, Oke A, DeRisi JL, Fung JC. ReCombine: a suite of programs for detection and analysis of meiotic recombination in whole-genome datasets. PloS one. 2011; 6:e25509. [PubMed: 22046241]

Anderson CM, Oke A, Yam P, Zhuge T, Fung JC. Reduced Crossover Interference and Increased ZMM-Independent Recombination in the Absence of Tel1/ATM. PLoS Genet. 2015; 11:e1005478. [PubMed: 26305689]

Argueso JL, Wanat J, Gemici Z, Alani E. Competing crossover pathways act during meiosis in Saccharomyces cerevisiae. Genetics. 2004; 168:1805–1816. [PubMed: 15611158]

Benjamin KR, Zhang C, Shokat KM, Herskowitz I. Control of landmark events in meiosis by the CDK Cdc28 and the meiosis-specific kinase Ime2. Genes Dev. 2003; 17:1524–1539. [PubMed: 12783856]

Blanco MG, Matos J, West SC. Dual control of Yen1 nuclease activity and cellular localization by Cdk and Cdc14 prevents genome instability. Mol Cell. 2014; 54:94–106. [PubMed: 24631285]

Borner GV, Kleckner N, Hunter N. Crossover/noncrossover differentiation, synaptonemal complex formation, and regulatory surveillance at the leptotene/zygotene transition of meiosis. Cell. 2004; 117:29–45. [PubMed: 15066280]

Chen SY, Tsubouchi T, Rockmill B, Sandler JS, Richards DR, Vader G, Hochwagen A, Roeder GS, Fung JC. Global analysis of the meiotic crossover landscape. Dev Cell. 2008; 15:401–415. [PubMed: 18691940]

Chu S, Herskowitz I. Gametogenesis in yeast is regulated by a transcriptional cascade dependent on Ndt80. Mol Cell. 1998; 1:685–696. [PubMed: 9660952]

Clyne RK, Katis VL, Jessop L, Benjamin KR, Herskowitz I, Lichten M, Nasmyth K. Polo-like kinase Cdc5 promotes chiasmata formation and cosegregation of sister centromeres at meiosis I. Nature cell biology. 2003; 5:480–485. [PubMed: 12717442]

Dayani Y, Simchen G, Lichten M. Meiotic recombination intermediates are resolved with minimal crossover formation during return-to-growth, an analogue of the mitotic cell cycle. PLoS Genet. 2011; 7:e1002083. [PubMed: 21637791]

de los Santos T, Hunter N, Lee C, Larkin B, Loidl J, Hollingsworth NM. The Mus81/Mms4 endonuclease acts independently of double-Holliday junction resolution to promote a distinct subset of crossovers during meiosis in budding yeast. Genetics. 2003; 164:81–94. [PubMed: 12750322]

De Muyt A, Jessop L, Kolar E, Sourirajan A, Chen J, Dayani Y, Lichten M. BLM helicase ortholog Sgs1 is a central regulator of meiotic recombination intermediate metabolism. Mol Cell. 2012; 46:43–53. [PubMed: 22500736]

Dehe PM, Gaillard PH. Control of structure-specific endonucleases to maintain genome stability. Nature reviews. Molecular cell biology. 2017; 18:315–330. [PubMed: 28327556]

Duroc Y, Kumar R, Ranjha L, Adam C, Guerois R, Md Muntaz K, Marsolier-Kergoat MC, Dingli F, Laureau R, Loew D, et al. Concerted action of the MutLbeta heterodimer and Mer3 helicase regulates the global extent of meiotic gene conversion. eLife. 2017; 6

Eissler CL, Mazon G, Powers BL, Savinov SN, Symington LS, Hall MC. The Cdk/cDc14 module controls activation of the Yen1 holliday junction resolvase to promote genome stability. Mol Cell. 2014; 54:80–93. [PubMed: 24631283]

Fung JC, Rockmill B, Odell M, Roeder GS. Imposition of crossover interference through the nonrandom distribution of synapsis initiation complexes. Cell. 2004; 116:795–802. [PubMed: 15035982]

Hassold T, Hunt P. To err (meiotically) is human: the genesis of human aneuploidy. Nat Rev Genet. 2001; 2:280–291. [PubMed: 11283700]

Hunter N. Meiotic Recombination: The Essence of Heredity. Cold Spring Harbor perspectives in biology. 2015; 7

Hunter N, Borts RH. Mlh1 is unique among mismatch repair proteins in its ability to promote crossing-over during meiosis. Genes Dev. 1997; 11:1573–1582. [PubMed: 9203583]

Hunter N, Kleckner N. The single-end invasion: an asymmetric intermediate at the double-strand break to double-holliday junction transition of meiotic recombination. Cell. 2001; 106:59–70. [PubMed: 11461702]

Ip SC, Rass U, Blanco MG, Flynn HR, Skehel JM, West SC. Identification of Holliday junction resolvases from humans and yeast. Nature. 2008; 456:357–361. [PubMed: 19020614]

Jessop L, Lichten M. Mus81/Mms4 endonuclease and Sgs1 helicase collaborate to ensure proper recombination intermediate metabolism during meiosis. Mol Cell. 2008; 31:313–323. [PubMed: 18691964]

Keeney S, Giroux CN, Kleckner N. Meiosis-specific DNA double-strand breaks are catalyzed by Spo11, a member of a widely conserved protein family. Cell. 1997; 88:375–384. [PubMed: 9039264]

Khazanehdari KA, Borts RH. EXO1 and MSH4 differentially affect crossing-over and segregation. Chromosoma. 2000; 109:94–102. [PubMed: 10855499]

Kim KP, Weiner BM, Zhang L, Jordan A, Dekker J, Kleckner N. Sister cohesion and structural axis components mediate homolog bias of meiotic recombination. Cell. 2010; 143:924–937. [PubMed: 21145459]

Knop M, Siegers K, Pereira G, Zachariae W, Winsor B, Nasmyth K, Schiebel E. Epitope tagging of yeast strains using a PCR-based strategy: more tags and improved prctical routines. Yeast. 1999; 15:963–972. [PubMed: 10407276]

Lee BH, Amon A. Role of Polo-like kinase Cdc5 in programming meiosis I chromosome segregation. Science. 2003; 300:482–486. [PubMed: 12663816]

Lorenz A, Osman F, Sun W, Nandi S, Steinacher R, Whitby MC. The fission yeast FANCM ortholog directs non-crossover recombination during meiosis. Science. 2012; 336:1585–1588. [PubMed: 22723423]

Lynn A, Soucek R, Borner GV. ZMM proteins during meiosis: crossover artists at work. Chromosome research : an international journal on the molecular, supramolecular and evolutionary aspects of chromosome biology. 2007; 15:591–605.

Mancera E, Bourgon R, Brozzi A, Huber W, Steinmetz LM. High-resolution mapping of meiotic crossovers and non-crossovers in yeast. Nature. 2008; 454:479–485. [PubMed: 18615017]

Manhart CM, Ni X, White MA, Ortega J, Surtees JA, Alani E. The mismatch repair and meiotic recombination endonuclease Mlh1-Mlh3 is activated by polymer formation and can cleave DNA substrates in trans. PLoS biology. 2017; 15:e2001164. [PubMed: 28453523]

Matos J, Blanco MG, Maslen S, Skehel JM, West SC. Regulatory control of the resolution of DNA recombination intermediates during meiosis and mitosis. Cell. 2011; 147:158–172. [PubMed: 21962513]

Matos J, Lipp JJ, Bogdanova A, Guillot S, Okaz E, Junqueira M, Shevchenko A, Zachariae WG. Dbf4-dependent Cdc7 kinase links DNA replication to the segregation of homologous chromosomes in meiosis I. Cell. 2008; 135:662–678. [PubMed: 19013276]

Medhi D, Goldman AS, Lichten M. Local chromosome context is a major determinant of crossover pathway biochemistry during budding yeast meiosis. eLife. 2016; 5

Muller HJ. The Mechanism of Crossing-Over. The American Naturalist. 1916; 50:193–221.

Nishant KT, Plys AJ, Alani E. A mutation in the putative MLH3 endonuclease domain confers a defect in both mismatch repair and meiosis in Saccharomyces cerevisiae. Genetics. 2008; 179:747–755. [PubMed: 18505871]

O'Neil NJ, Martin JS, Youds JL, Ward JD, Petalcorin MI, Rose AM, Boulton SJ. Joint molecule resolution requires the redundant activities of MUS-81 and XPF-1 during Caenorhabditis elegans meiosis. PLoS Genet. 2013; 9:e1003582. [PubMed: 23874209]

Oh SD, Lao JP, Hwang PY, Taylor AF, Smith GR, Hunter N. BLM ortholog, Sgs1, prevents aberrant crossing-over by suppressing formation of multichromatid joint molecules. Cell. 2007; 130:259–272. [PubMed: 17662941]

Oke A, Anderson CM, Yam P, Fung JC. Controlling meiotic recombinational repair - specifying the roles of ZMMs, Sgs1 and Mus81/Mms4 in crossover formation. PLoS Genet. 2014; 10:e1004690. [PubMed: 25329811]

Osman F, Dixon J, Doe CL, Whitby MC. Generating crossovers by resolution of nicked Holliday junctions: a role for Mus81-Eme1 in meiosis. Mol Cell. 2003; 12:761–774. [PubMed: 14527420]

Padmore R, Cao L, Kleckner N. Temporal comparison of recombination and synaptonemal complex formation during meiosis in S. cerevisiae. Cell. 1991; 66:1239–1256. [PubMed: 1913808]

Petronczki M, Matos J, Mori S, Gregan J, Bogdanova A, Schwickart M, Mechtler K, Shirahige K, Zachariae W, Nasmyth K. Monopolar attachment of sister kinetochores at meiosis I requires casein kinase 1. Cell. 2006; 126:1049–1064. [PubMed: 16990132]

Ranjha L, Anand R, Cejka P. The Saccharomyces cerevisiae Mlh1-Mlh3 heterodimer is an endonuclease that preferentially binds to Holliday junctions. J Biol Chem. 2014; 289:5674–5686. [PubMed: 24443562]

Rogacheva MV, Manhart CM, Chen C, Guarne A, Surtees J, Alani E. Mlh1-Mlh3, a meiotic crossover and DNA mismatch repair factor, is a Msh2-Msh3-stimulated endonuclease. J Biol Chem. 2014; 289:5664–5673. [PubMed: 24403070]

Saito TT, Lui DY, Kim HM, Meyer K, Colaiacovo MP. Interplay between structure-specific endonucleases for crossover control during Caenorhabditis elegans meiosis. PLoS Genet. 2013; 9:e1003586. [PubMed: 23874210]

Salah SM, Nasmyth K. Destruction of the securin Pds1p occurs at the onset of anaphase during both meiotic divisions in yeast. Chromosoma. 2000; 109:27–34. [PubMed: 10855492]

Schwacha A, Kleckner N. Identification of joint molecules that form frequently between homologs but rarely between sister chromatids during yeast meiosis. Cell. 1994; 76:51–63. [PubMed: 8287479]

Schwacha A, Kleckner N. Identification of double Holliday junctions as intermediates in meiotic recombination. Cell. 1995; 83:783–791. [PubMed: 8521495]

Shah Punatar R, Martin MJ, Wyatt HD, Chan YW, West SC. Resolution of single and double Holliday junction recombination intermediates by GEN1. Proc Natl Acad Sci U S A. 2017; 114:443–450. [PubMed: 28049850]

Smith GR, Boddy MN, Shanahan P, Russell P. Fission yeast Mus81.Eme1 Holliday junction resolvase is required for meiotic crossing over but not for gene conversion. Genetics. 2003; 165:2289–2293. [PubMed: 14704204]

Snowden T, Acharya S, Butz C, Berardini M, Fishel R. hMSH4-hMSH5 recognizes Holliday Junctions and forms a meiosis-specific sliding clamp that embraces homologous chromosomes. Mol Cell. 2004; 15:437–451. [PubMed: 15304223]

Sourirajan A, Lichten M. Polo-like kinase Cdc5 drives exit from pachytene during budding yeast meiosis. Genes Dev. 2008; 22:2627–2632. [PubMed: 18832066]

Storici F, Resnick MA. Delitto perfetto targeted mutagenesis in yeast with oligonucleotides. Genet Eng (N Y). 2003; 25:189–207. [PubMed: 15260239]

Sun H, Treco D, Szostak JW. Extensive 3'-overhanging, single-stranded DNA associated with the meiosis-specific double-strand breaks at the ARG4 recombination initiation site. Cell. 1991; 64:1155–1161. [PubMed: 2004421]

Thacker D, Lam I, Knop M, Keeney S. Exploiting spore-autonomous fluorescent protein expression to quantify meiotic chromosome behaviors in Saccharomyces cerevisiae. Genetics. 2011; 189:423–439. [PubMed: 21840861]

Toth A, Rabitsch KP, Galova M, Schleiffer A, Buonomo SB, Nasmyth K. Functional genomics identifies monopolin: a kinetochore protein required for segregation of homologs during meiosis i. Cell. 2000; 103:1155–1168. [PubMed: 11163190]

Tung KS, Hong EJ, Roeder GS. The pachytene checkpoint prevents accumulation and phosphorylation of the meiosis-specific transcription factor Ndt80. Proc Natl Acad Sci U S A. 2000; 97:12187–12192. [PubMed: 11035815]

Wang S, Hassold T, Hunt P, White MA, Zickler D, Kleckner N, Zhang L. Inefficient Crossover Maturation Underlies Elevated Aneuploidy in Human Female Meiosis. Cell. 2017; 168:977–989. e917. [PubMed: 28262352]

Wang TF, Kleckner N, Hunter N. Functional specificity of MutL homologs in yeast: evidence for three Mlh1-based heterocomplexes with distinct roles during meiosis in recombination and mismatch correction. Proc Natl Acad Sci U S A. 1999; 96:13914–13919. [PubMed: 10570173]

West SC, Blanco MG, Chan YW, Matos J, Sarbajna S, Wyatt HD. Resolution of Recombination Intermediates: Mechanisms and Regulation. Cold Spring Harbor symposia on quantitative biology. 2015

Yildiz O, Majumder S, Kramer B, Sekelsky JJ. Drosophila MUS312 interacts with the nucleotide excision repair endonuclease MEI-9 to generate meiotic crossovers. Mol Cell. 2002; 10:1503–1509. [PubMed: 12504024]

Zakharyevich K, Ma Y, Tang S, Hwang PY, Boiteux S, Hunter N. Temporally and biochemically distinct activities of Exo1 during meiosis: double-strand break resection and resolution of double Holliday junctions. Mol Cell. 2010; 40:1001–1015. [PubMed: 21172664]

Zakharyevich K, Tang S, Ma Y, Hunter N. Delineation of joint molecule resolution pathways in meiosis identifies a crossover-specific resolvase. Cell. 2012; 149:334–347. [PubMed: 22500800]

Zelazowski MJ, Sandoval M, Paniker L, Hamilton HM, Han J, Gribbell MA, Kang R, Cole F. Age-Dependent Alterations in Meiotic Recombination Cause Chromosome Segregation Errors in Spermatocytes. Cell. 2017; 171:601–614. e613. [PubMed: 28942922]

Zhang L, Wang S, Yin S, Hong S, Kim KP, Kleckner N. Topoisomerase II mediates meiotic crossover interference. Nature. 2014; 511:551–556. [PubMed: 25043020]

Zickler D, Kleckner N. A few of our favorite things: Pairing, the bouquet, crossover interference and evolution of meiosis. Seminars in cell & developmental biology. 2016; 54:135–148. [PubMed: 26927691]

HIGHLIGHTS

- Yen1 phosphorylation avoids its pervasive recruitment to meiotic HR intermediates
- Active inhibition of Yen1 prevents untimely resolution of DNA joint molecules
- Temporal control of DNA joint molecule resolution enables crossover patterning
- Meiotic properties of DNA joint molecules support crossover-specific resolution

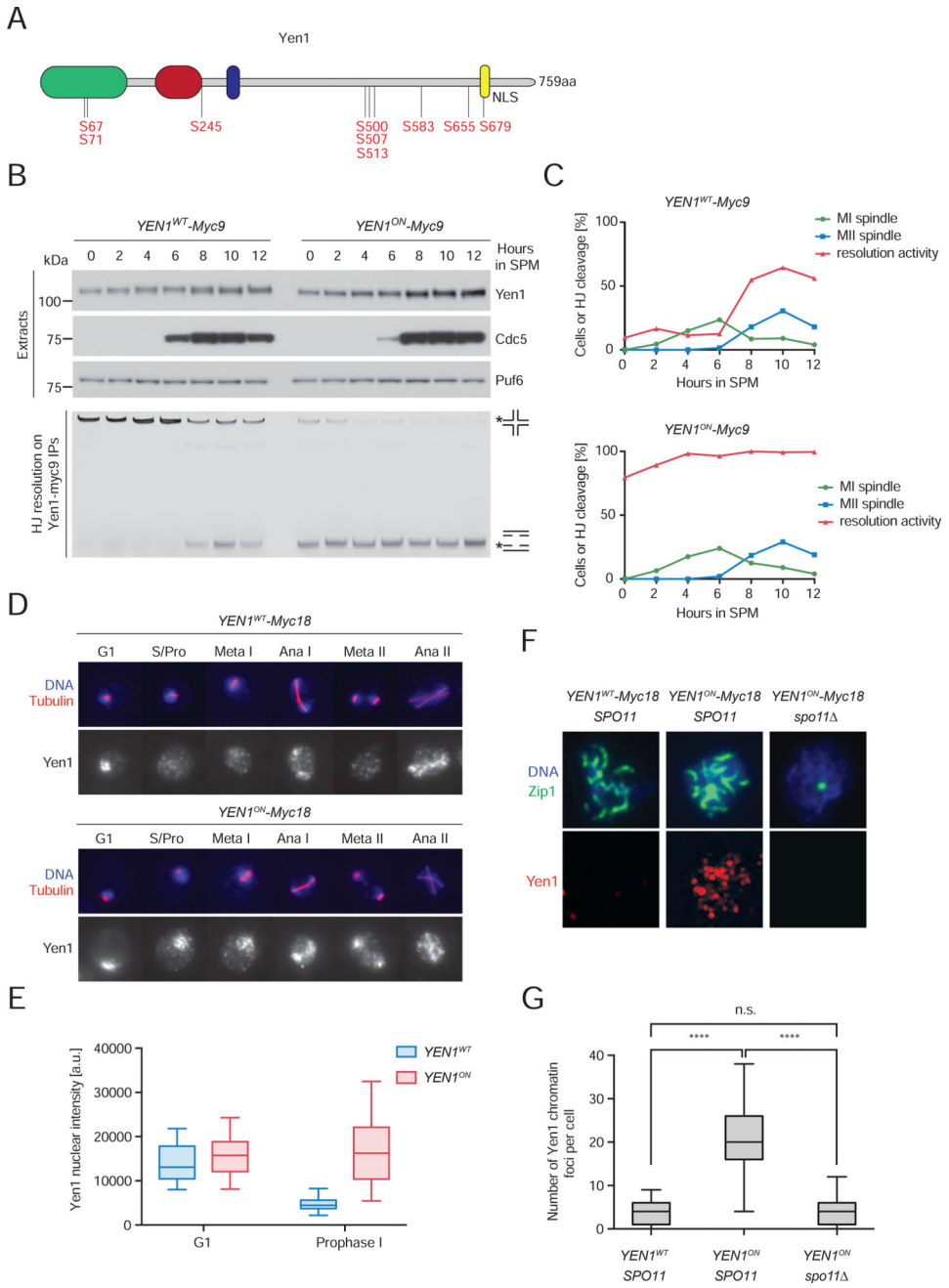

Figure 1. Inhibitory phosphorylation regulates the biochemical activity, nuclear localization and chromatin recruitment of Yen1 during meiosis. See also Figure S1

(**A**) Schematic representation of Yen1, highlighting the nine serine residues at Ser-Pro sites subject to inhibitory phosphorylation by Cdk1.

(**B**) Analysis of expression levels and nuclease activity of Yen1^{WT} and Yen1^{ON} during meiosis. Soluble extracts were prepared from *YEN1^{WT}-Myc9* and *YEN1^{ON}-Myc9* strains at 2-hr intervals after transfer into sporulation medium (SPM). Following anti-Myc immunoaffinity purification (IP), the IPs were analyzed by western blotting and tested for nuclease activity using Cy3-labeled Holliday junction DNA as a substrate. Upper panel: western blots of the cell extracts, with detection of Yen1-myc9, Cdc5 and Puf6 (loading

control). Lower panel: HJ resolution assay. The experiment shown is representative of 3 independent experiments.

(**C**) Quantification of Yen1 HJ resolvase activity relative to the kinetics of meiotic progression as determined from (**B**). %HJ cleavage (red) was calculated by dividing the relative signal of nicked-duplex DNA product by the sum of cleaved product and intact HJ DNA. Spindle morphology was determined by IF analysis of anti-tubulin from samples collected at the indicated times after induction of meiosis. Meiosis I cells had a single bipolar spindle (MI spindle, green) while meiosis II cells had two bipolar spindles (MII spindle, blue). 200 cells were analyzed per time point.

(**D**) Representative images of the subcellular localization of $Yen1^{WT}$ and $Yen1^{ON}$ throughout meiosis. Yen1-myc18 expressed from the endogenous promoter was analyzed by immunofluorescence using anti-Myc antibodies. Spindle morphology and DNA were visualized using anti-tubulin antibodies and DAPI. The experiment shown is representative of 2 independent experiments.

(**E**) Quantitative analysis of the integrated nuclear intensity of $Yen1^{WT}$ and $Yen1^{ON}$ from (**D**). Comparison of Yen1 signal in the nuclei of G1 and prophase I cells. Tukey box plots depict median intensity with whiskers representing upper and lower 1.5 inter-quartile range. 25 cells were analyzed per condition.

(**F**) Chromosome spreads from strains expressing myc18-tagged $Yen1^{WT}$ or $Yen1^{ON}$ were prepared 7 hrs after induction of meiosis and stained for DNA, Zip1 and Yen1-myc18. Prophase I cells were identified by full Zip1 loading. In cells lacking *SPO11*, prophase I cells were identified by having a strong Zip1 polycomplex. Representative images are shown.

(**G**) Analysis of Yen1 foci number in chromosome spreads from (**F**). Tukey box plots depict median number of Yen1 foci with whiskers representing upper and lower 1.5 inter-quartile range. 35 cells were analyzed per condition (one-way ANOVA, $F(2,102)=130.6$, $P<0.0001$ followed by Tukey's Multiple Comparison Test, ****$p<0.0001$; n.s., not significant). The experiment shown is representative of 2 independent experiments.

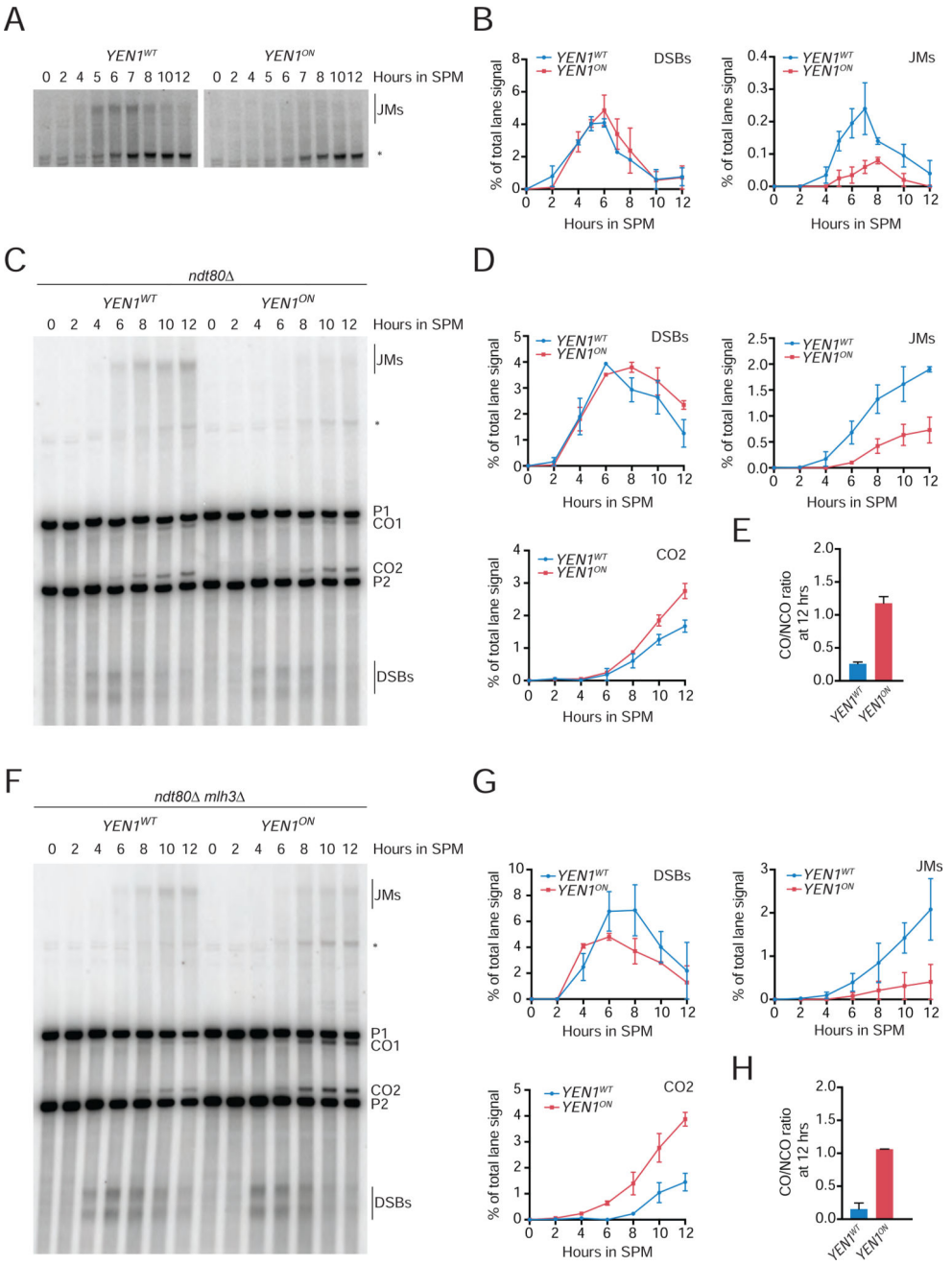

Figure 2. Phosphorylation-resistant Yen1 resolves recombination intermediates prematurely. See also Figure S2

(**A**) Physical analysis of recombination at the *HIS4-LEU2* locus in cells expressing either *YEN1*^{WT} or *YEN1*^{ON} from the endogenous promoter. Cells were collected at the indicated time intervals after transfer into sporulation medium (SPM). Psoralen-crosslinked DNA prepared from the meiotic time courses was analyzed by Southern blotting. JM: joint molecules; asterisk indicates ectopic crossovers. Images are representative of 2 independent experiments.

(**B**) DNA double-strand break (DSB) formation and JM accumulation were quantified as fractions of the total lane signal from Figure S2B and from (A). Plotted values show the

mean of two independent experiments; error bars represent range. Panels in (A) and S2B are cropped from the top (A) and bottom (S2B) of the same gel but shown separately due to the need for different exposures. Quantifications were performed from the same exposure.

(**C**) Physical analysis of recombination at *HIS4-LEU2* in *ndt80Δ* strains expressing either $YEN1^{WT}$ or $YEN1^{ON}$ from the endogenous promoter. JMs, joint molecules; P1, parental DNA 1; P2, parental DNA 2; CO1 and CO2, reciprocal recombinants from P1 and P2; DSBs, double-strand breaks. Images are representative of 2 independent experiments.

(**D**) DSB, JM and CO2 accumulation were quantified from (C) and from a biological replicate as in (B).

(**E**) CO/NCO ratio after 12 hrs in SPM was calculated from data in Figure S2F; error bars represent range in two independent experiments.

(**F**) Physical analysis of recombination as in (C), in *ndt80Δ mlh3Δ* cells expressing either $YEN1^{WT}$ or $YEN1^{ON}$ from the endogenous promoter.

(**G**) DSB, JM and CO2 accumulation were quantified from (F) and from a biological replicate as in (B).

(**H**) CO/NCO ratio after 12 hrs in SPM was calculated from data in Figure S2I as in (E).

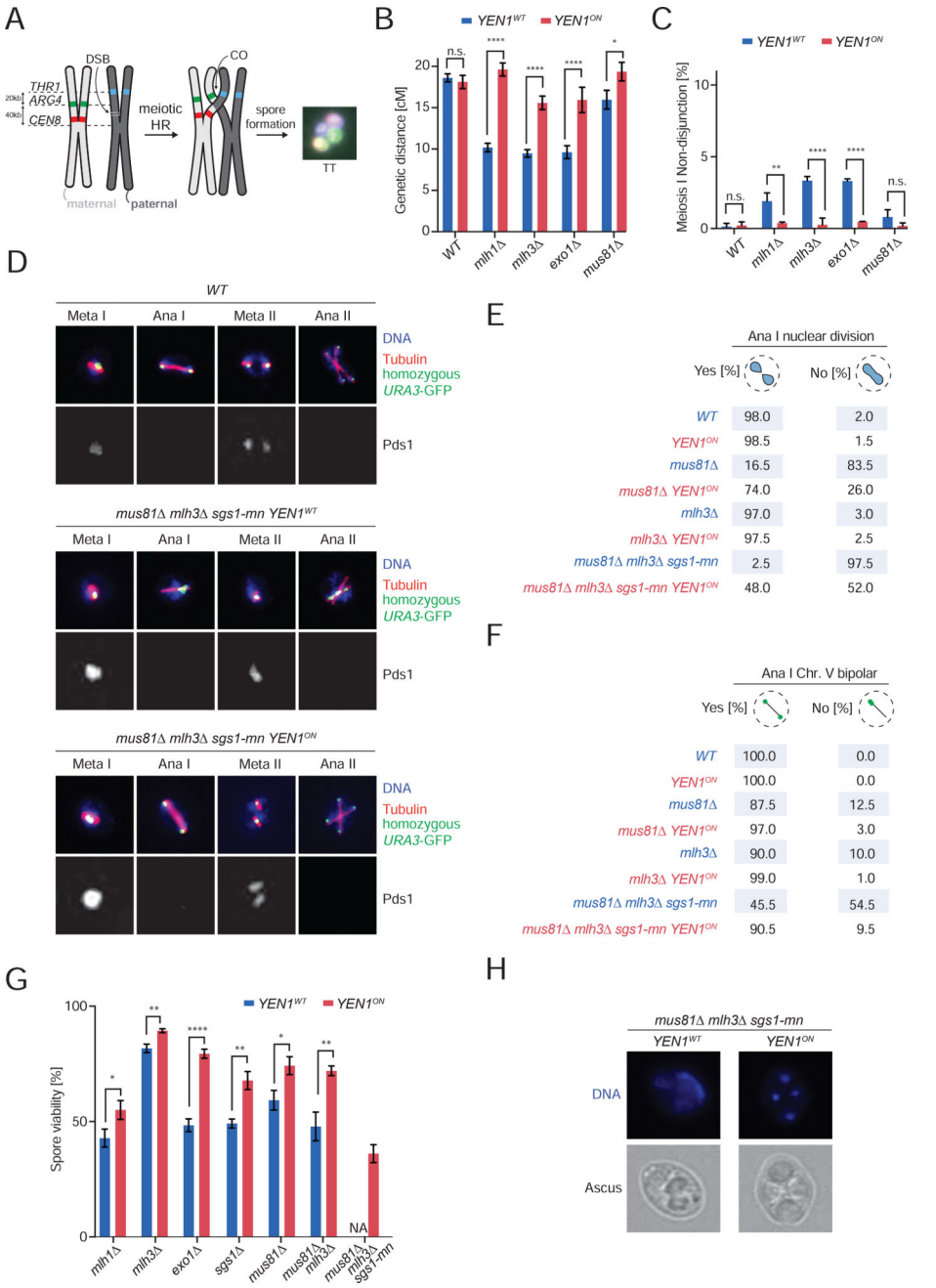

Figure 3. Yen1^{ON} improves crossover formation, chromosome segregation and spore viability in mutants defective in joint molecule processing. See also Figure S3

(**A**) Schematic representation of a live-cell reporter assay to measure crossover (CO) recombination and interference at *CEN8-THR1*. Homologous chromosomes are shown in light and dark grey with GFP, tdTomato and CFP reporters represented in green, red and cyan, respectively. A micrograph and illustration of the marker conFiguration when there is one recombination event in the *CEN8-ARG4* interval is shown. Marker conFigurations that reflect formation of alternative COs or meiosis I non-disjunction events are depicted in Figure S3A. TT, tetratype.

(**B**) Meiosis was induced in liquid cultures of the indicated genotypes and spore formation was allowed to occur for 48 hrs at 30°C. Genetic distances at the *CEN8-THR1* interval were determined using the fluorescent markers described in (A). >720 tetrads were analyzed in two to four independent experiments. Plotted values indicate mean +/− SEM (two-tailed, unpaired t-test, *p<0.05, ****p<0.0001, n.s., non-significant). The raw data for this experiment is described in Figure S3B.

(**C**) Estimated frequency of meiosis I non-disjunction in strains from (B). Plotted values indicate mean +/− SEM (two-tailed, unpaired t-test, **p<0.01, ****p<0.0001, n.s., non-significant).

(**D**) $YEN1^{ON}$ restores chromosome segregation in mutants defective in JM resolution. Immunofluorescence analysis of strains expressing Pds1-myc18 (for securin visualization) and carrying *URA3*-GFP (GFP marks chromosome V at *URA3*) in the indicated backgrounds. Representative images taken at different stages of the cell cycle illustrate chromosome segregation patterns.

(**E**) Frequency of nuclear division, assayed by DAPI staining of DNA, during anaphase I (Ana I), from cells in (D). 200 cells were analyzed per condition. Ana I was defined by the presence of a bipolar spindle and absence of Pds1 staining.

(**F**) Frequency of chromosome V segregation, assayed by GFP fluorescence, during anaphase I (Ana I), from cells in (D). 200 cells were analyzed per condition. Ana I was defined by the presence of a bipolar spindle and absence of Pds1 staining.

(**G**) $YEN1^{ON}$ improves spore viability in mutants defective in JM processing and CO formation. Spore viability was measured 24 hrs after induction of meiosis on SPM plates, at 30°C. 432 spores were analyzed per genotype in six independent experiments. NA, *mus81Δ mlh3Δ sgs1-mn* triple mutants sporulate but do not form dissectable tetrads. (mean +/− SEM, two-tailed, unpaired t-test, *p<0.05, **p<0.01, ****p<0.0001, n.s., non-significant).

(**H**) Representative asci and DAPI stained DNA in mutants with the indicated genotypes after completion of meiosis.

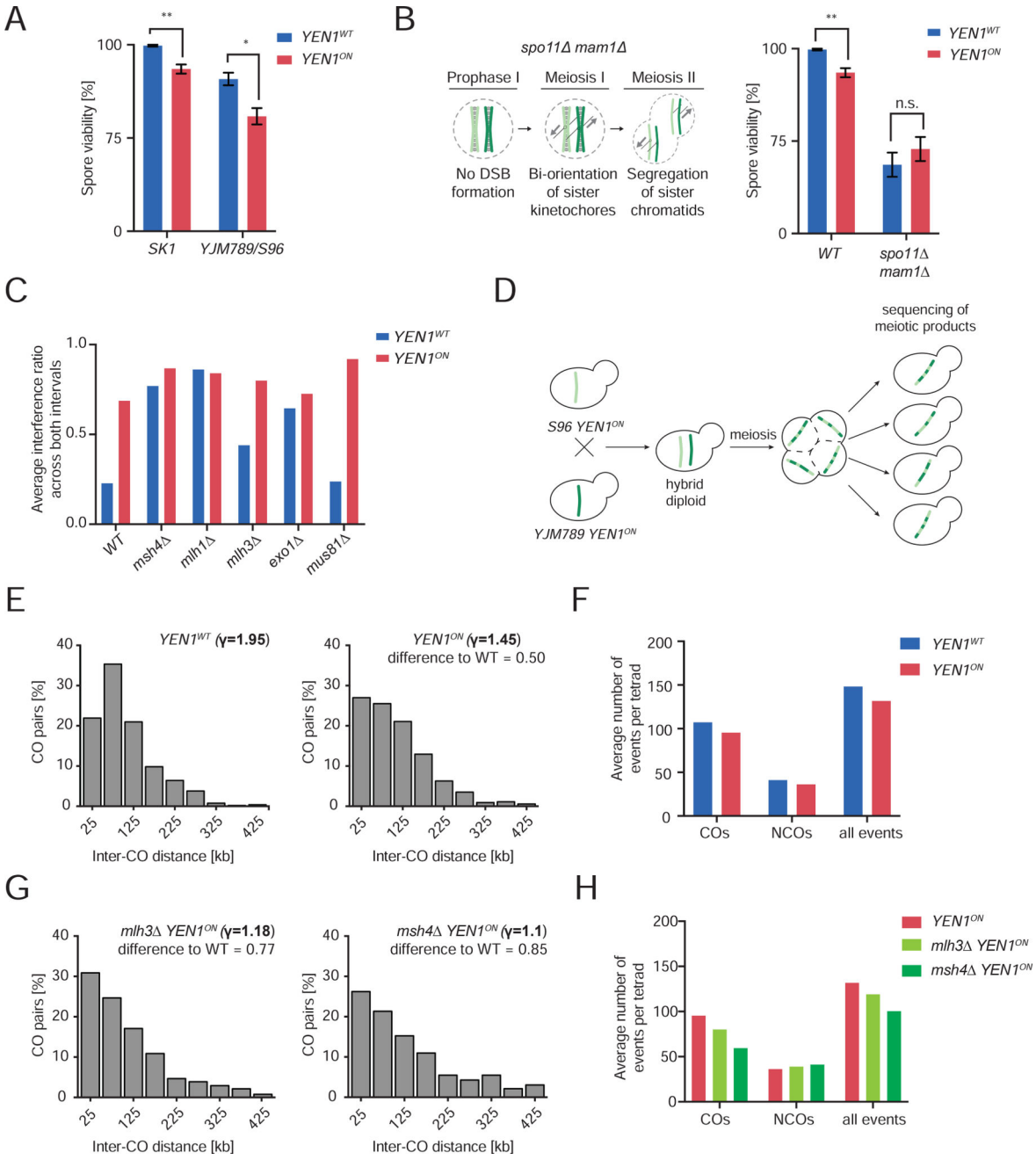

Figure 4. Yen1 activity during prophase I is deleterious to spore viability and impairs crossover distribution genome-wide. See also Figure S4

(**A**) Spore viability of strains with the indicated genotypes was measured 24 hrs (SK1 diploids) or 48 hrs (YJM789/S96 hybrids) after induction of meiosis on SPM plates, at 30°C. 432 spores were analyzed for SK1 diploids in 6 independent experiments and 408 spores were analyzed for the YJM789/S96 hybrid in 7 independent experiments (mean +/− SEM, two-tailed, unpaired t-test, *p<0.05,**p<0.01).

(**B**) Left panel: cartoon illustrating chromosome segregation in *spo11Δ mam1Δ* double mutants, which generate viable dyads without initiating meiotic recombination. Right panel: spore viability of strains with the indicated genotypes, as in (A). 432 spores were analyzed

per genotype in 6 independent experiments. Displayed data for wild-type SK1 diploids is from (A), **p<0.01, n.s., non-significant.

(**C**) CO interference was assessed using the 3-marker reporter system introduced in Figure 3A for strains with the indicated genotypes. >720 tetrads were analyzed in two to four independent experiments. The average interference ratios for the two intervals are plotted. A smaller ratio reflects a stronger apparent interference.

(**D**) Rationale of genome-wide mapping of recombination events by analysis of SNPs after sequencing of germinated spores resulting from hybrid meiosis.

(**E**) Histogram analysis of distances between adjacent COs in cells expressing $YEN1^{WT}$ or $YEN1^{ON}$ from the endogenous promoter. In wild-type cells, inter-CO distances are well fit by a gamma distribution. The value of the shape parameter γ of the best-fit distribution indicates the strength of interference, with $\gamma > 1$ indicating positive interference and $\gamma = 1$ indicating random distribution. 6 tetrads were analyzed for $YEN1^{WT}$ and 7 for $YEN1^{ON}$.

(**F**) Overall recombination levels are not affected in the $YEN1^{ON}$ mutant. Average number of COs, NCOs and all events (COs + NCOs) in $YEN1^{WT}$ and $YEN1^{ON}$ per tetrad are shown.

(**G**) Histogram analysis of distances of adjacent COs in cells with the indicated genotypes, as in (E). 8 tetrads were analyzed per genotype.

(**H**) Average number of COs, NCOs and all events (COs + NCOs) in the indicated strains, as in (F).

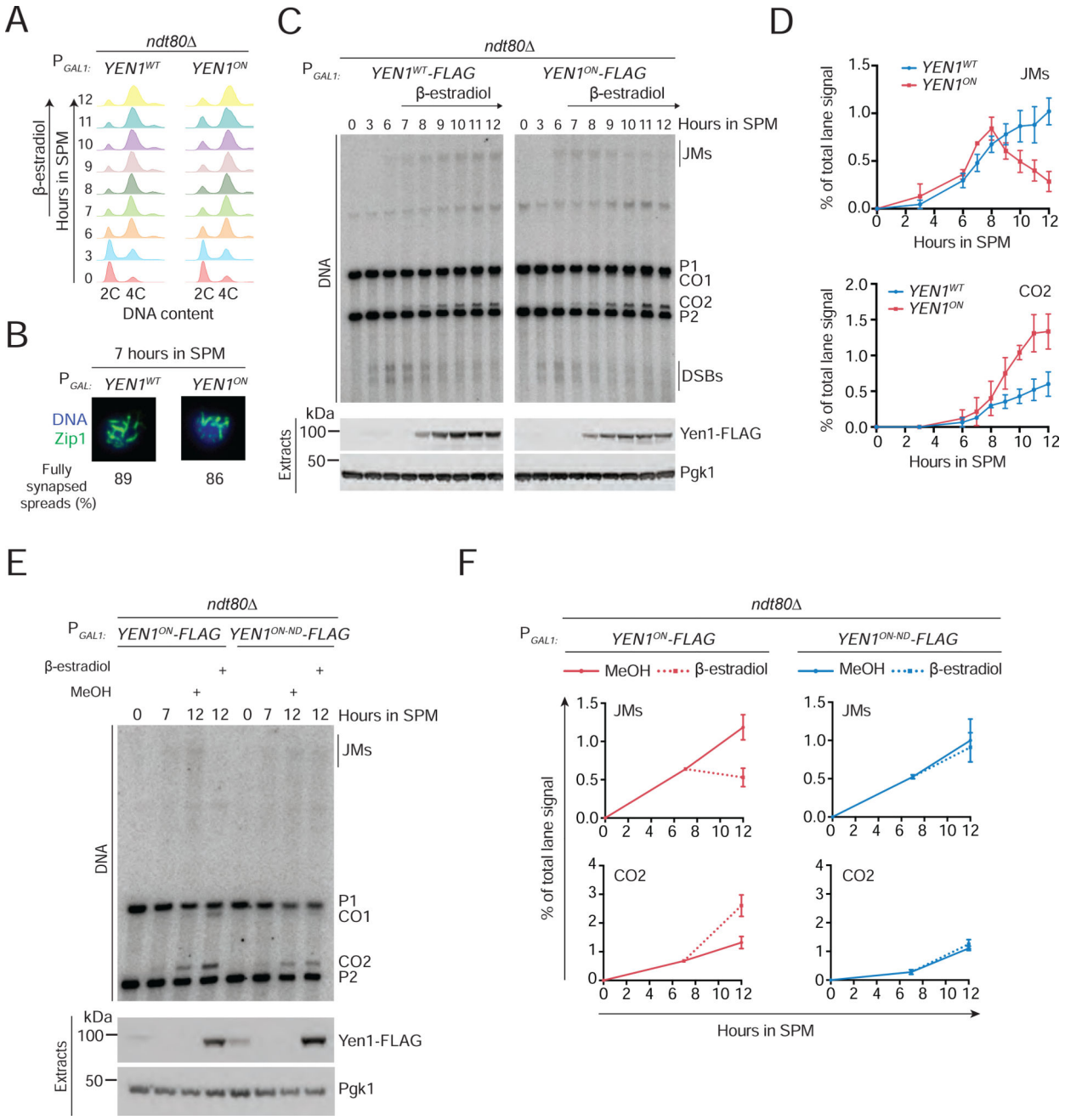

Figure 5. Resolution of ZMM-stabilized joint molecules by Yen1. See also Figure S5

(**A**) *ndt80Δ* P_{GPD}-*GAL4-ER* cells carrying *YEN1*^{WT}-*FLAG* or *YEN1*^{ON}-*FLAG* under the control of P_{GAL1} were synchronously released to undergo meiosis and arrest in pachytene. Yen1 expression was initiated 7 hrs after induction of meiosis by addition of β-estradiol. Samples were collected at the indicated time points and DNA content analyzed by FACS. (**B**) The efficiency of pachytene arrest at the time of Yen1 induction in (A) was verified by analysis of synaptonemal complex formation by Zip1 staining in chromosome spreads. (**C**) Physical analysis of recombination at the *HIS4-LEU2* locus (top panel) and western blot analysis of the indicated proteins (lower panels) were performed for cells in (A). Note: Yen1

levels are ~2-fold higher than endogenous expression of Yen1. The experiment shown is representative of 2 independent experiments.

(**D**) Dynamics of JM and CO2 accumulation were quantified from (C) and from a biological replicate. Plotted values show the mean of two independent experiments; error bars represent range.

(**E**) *ndt80Δ* P_{GPD}-*GAL4-ER* cells carrying *YEN1*^{ON}-*FLAG* or *YEN1*$^{ON\text{-}ND}$-*FLAG* under the control of P_{GAL1} were synchronously released to undergo meiosis and, 7hrs after transfer to SPM, divided in two. Half the culture was treated with MeOH (control induction) and the other half with β-estradiol (*YEN1*^{ON}-*FLAG* induction). Samples were collected at the indicated time points and analyzed as in (C). *YEN1*$^{ON\text{-}ND}$ is Nuclease-Dead due to the mutations E193A and E195A. The experiment shown is representative of 2 independent experiments.

(**F**) Dynamics of JM and CO2 accumulation were quantified from (E) and from a biological replicate, as in (D).

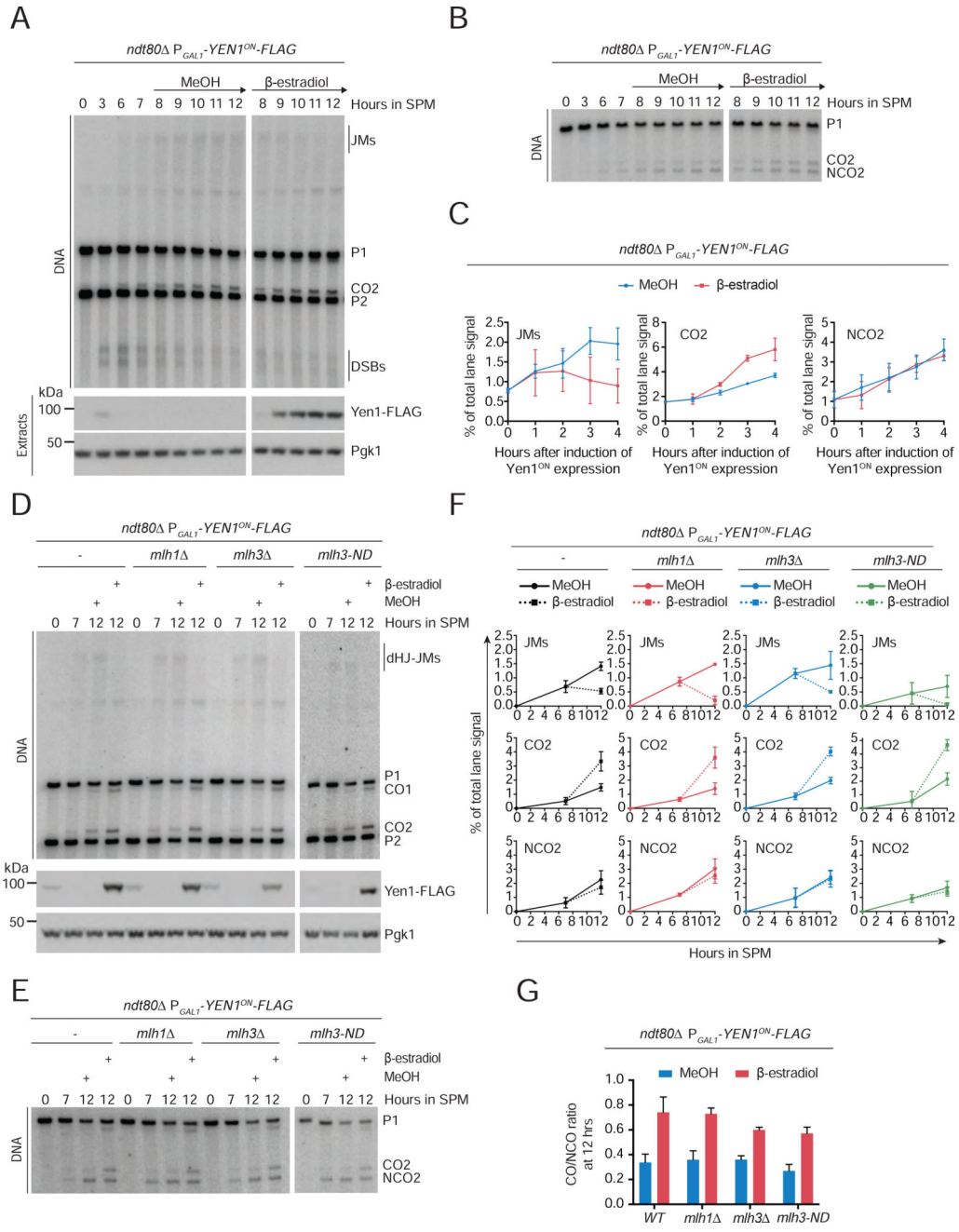

Figure 6. Crossover-specific resolution of DNA joint molecules by Yen1. See also Figure S6

(**A**) *ndt80Δ* P*GPD-GAL4-ER* cells carrying *YEN1ON-FLAG* under the control of P*GAL1* were synchronously released to undergo meiosis and arrest in pachytene. The culture was split 7 hrs after induction of meiosis and treated with MeOH (control induction) or β-estradiol (*YEN1ON-FLAG* induction). Samples were collected at the indicated time points and protein extracts analyzed by western-blotting for the indicated proteins (lower panels). Identical samples were treated with psoralen to crosslink DNA and the *HIS4-LEU2* locus was analyzed by Southern blotting (upper panels). The experiment shown is representative of 2 independent experiments.

(**B**) Southern blot of XhoI + NgoMIV double-digested genomic DNA prepared from cells in (A). CO2 (reciprocal recombinant from P1 and P2); NCO2 (non-crossover recombinant from P1 and P2).

(**C**) Dynamics of JM, CO2 and NCO2 accumulation were quantified from (A and B) and from biological replicates. Plotted values show the mean of two independent experiments; error bars represent range.

(**D**) Cells of the indicated genotypes were treated and analyzed as in (A). The experiment shown is representative of 2 independent experiments.

(**E**) Southern blot analysis of DNA prepared from cells in (D) as in (B).

(**F**) Dynamics of JM, CO2 and NCO2 accumulation were quantified from (D and E) as in (C).

(**G**) Quantification of the ratio of CO2 to NCO2 recombinants from XhoI + NgoMIV double-digests (E) of strains with the indicated genotypes. Plotted values are the mean of two independent experiments; error bars represent range.

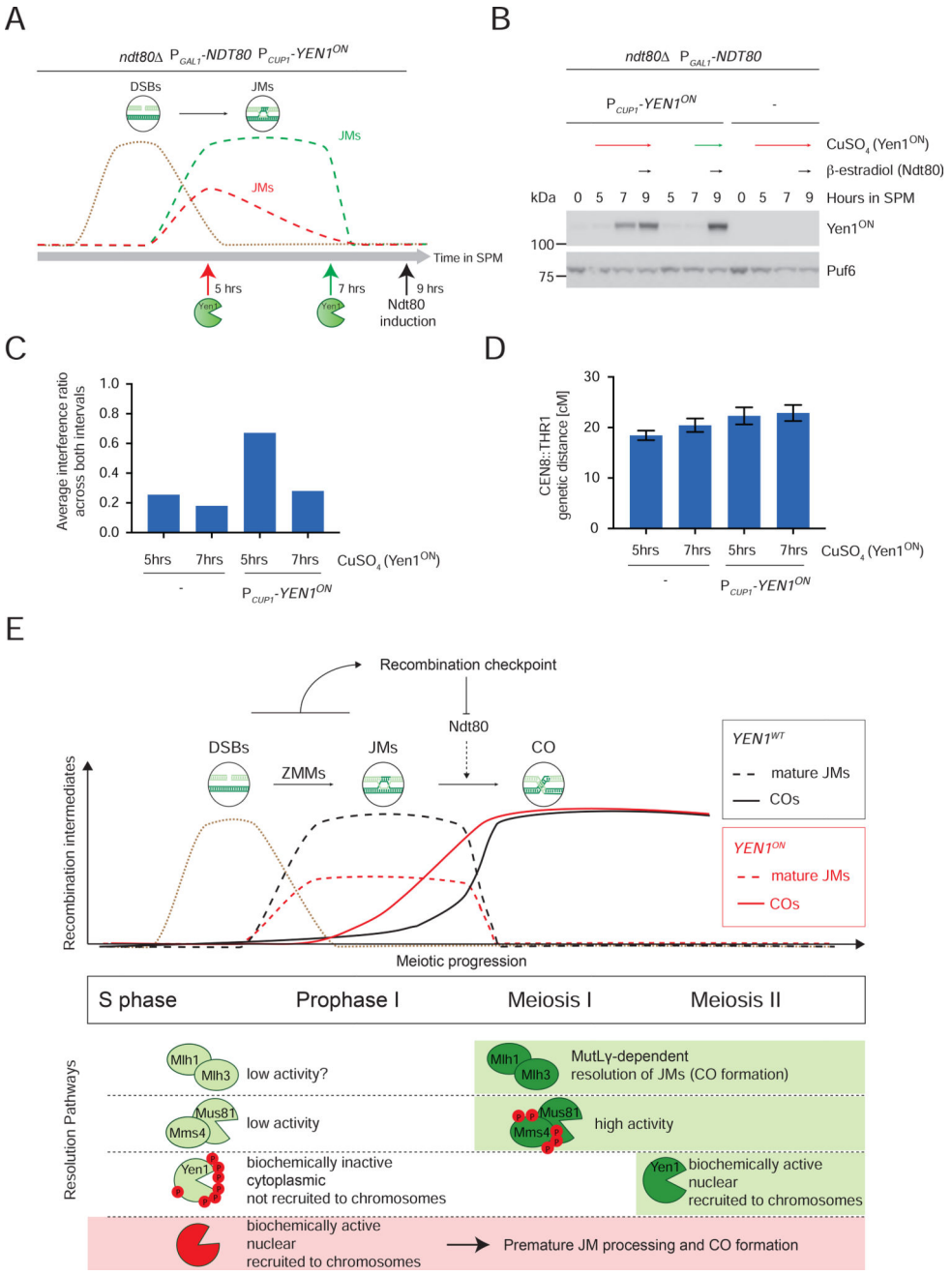

Figure 7. Pachytene-specific JM resolution by Yen1 does not interfere with spatial crossover distribution. See also Figure S7

(**A**) Scheme of Yen1^{ON} induction from P$_{CUP1}$ (P$_{CUP1}$-*YEN1^{ON}-Myc9*) at different time points during meiosis in a *ndt80Δ* strain containing P$_{GAL1}$-*NDT80*. After DNA replication is completed, 5 hrs after induction of meiosis, half of the culture is treated with 1 μM $CuSO_4$, to induce Yen1^{ON} expression as cells form joint molecules (JMs) (red arrow and curve). The other half is treated with $CuSO_4$ two hours later (7 hrs after induction of meiosis), to induce Yen1^{ON} expression after cells accumulate in pachytene (green arrow and curve). β-estradiol is added to both cultures 9 hrs after induction of meiosis to trigger Ndt80 expression and exit from pachytene.

(**B**) Stains carrying the live-cell reporter assay to measure CO recombination and interference at *CEN8-THR1* as well as P_{CUP1}-*YEN1*^{ON}-*Myc9* and P_{GAL1}-*NDT80* were treated as detailed in (A). A strain lacking P_{CUP1}-*YEN1*^{ON}-*Myc9* was used to control for potential side-effects of $CuSO_4$. Western blot samples were collected at the indicated time points to monitor for expression of Yen1^{ON}. The experiment shown is representative of 2 independent experiments.

(**C**) Spore formation was allowed to occur in cells from (B) for 48 hrs at 30°C. CO interference was assessed using the 3-marker reporter system introduced in Figure 3A. The average interference ratios for the two intervals are plotted. A smaller ratio reflects a stronger apparent interference. >430 tetrads were analyzed in 2 or 3 independent experiments. The raw data for this experiment is described in Figure S7B.

(**D**) Genetic distances at the *CEN8-THR1* interval in cells from (C) were determined using the fluorescent markers described in Figure 3A. Plotted values indicate mean +/− SEM.

(**E**) ZMMs stabilize nascent joint molecules (JMs) arising from the repair of DNA double-strand breaks (DSBs). Expression of the transcription factor Ndt80, which is negatively regulated by the recombination checkpoint, triggers JM resolution and crossover (CO) formation. Upper panel: schematic representation of the accumulation of different recombination intermediates in cells carrying *YEN1*^{WT} (black) or *YEN1*^{ON} (red). Lower panel: dynamic activation of different pathways of JM resolution establishes a hierarchy in pathway usage. Premature activation of a SSE - as depicted for Yen1, by Yen1^{ON} - prevents JM accumulation, leading to defects in the spatial distribution of COs.

KEY RESOURCES TABLE

REAGENT or RESOURCE	SOURCE	IDENTIFIER
Antibodies		
Rat monoclonal anti-tubulin	Serotec	Cat#MCA78G
Rabbit polyclonal anti-Zip1	Santa Cruz	Cat#sc-33733
Rabbit polyclonal anti-Myc	Santa Cruz	Cat#sc-789
Donkey anti-Rat IgG Alexa Fluor 488	Invitrogen	Cat#A-21208
Goat anti-Rabbit IgG Alexa Fluor 546	Invitrogen	Cat#A-11010
Donkey anti-Rabbit IgG Alexa Fluor 488	Invitrogen	Cat#A-21206
Donkey anti-Mouse IgG Alexa Fluor 555	Invitrogen	Cat#A-31570
Donkey anti-Mouse IgG Alexa Fluor 647	Invitrogen	Cat#A-31571
Goat anti-Rat IgG Alexa Fluor 568	Invitrogen	Cat#A-11077
Rabbit polyclonal anti-Myc (HRP)	Abcam	Cat#ab1326
Mouse monoclonal anti-FLAG (HRP)	Sigma Aldrich	Cat#a8592
Goat polyclonal anti-Cdc5	Santa Cruz	Cat#sc-6732
Mouse monoclonal anti-Pgk1	Invitrogen	Cat#459250
Rabbit anti-Puf6	V. Panse	N/A
Mouse monoclonal anti-Myc 9E10	Cancer Research UK	N/A
Chemicals, Peptides, and Recombinant Proteins		
β-Estradiol	Sigma Aldrich	Cat#E8875
Copper(II) sulfate	Sigma Aldrich	Cat#61230
Trioxsalen	Sigma Aldrich	Cat#T6137
ProLong™ Diamond Antifade Mountant with DAPI	Thermo Fisher	Cat#P36962
NuPAGE sample buffer	Thermo Fisher	Cat#NP0008
cOmplete™ protease inhibitor cocktail	Roche	Cat#05056489001
Critical Commercial Assays		
AminoLink™ Plus Immobilization Kit	Thermo Fisher	Cat#44894
Qubit dsDNA broad range kit	Thermo Fisher	Cat#Q32850
Deposited Data		
Sequencing datasets	NIH Sequence Read Archive	SRP144029
Experimental Models: Organisms/Strains		
S. cerevisiae SK1 *MATalpha ho::LYS2 ura3 leu2::hisG trp1::hisG his3::hisG*	W. Zachariae	WZ848, YML3
S. cerevisiae SK1 *MATa ho::LYS2 ura3 leu2::hisG trp1::hisG his3::hisG*	Matos lab	YML560
SK1 *MATa/MATalpha YEN1-myc9::KITRP1*	This study	YML4335
SK1 *MATa/MATalpha YEN1^{ON}-myc9::KITRP1*	This study	YML4337
SK1 *MATa/MATalpha YEN1-myc18::URA3*	This study	YML3952
SK1 *MATa/MATalpha YEN1^{ON} -myc18::URA3*	This study	YML3888
SK1 *MATa/MATalpha YEN1^{ON} -myc18::URA3 spo11Δ::URA3*	This study	YML3889

REAGENT or RESOURCE	SOURCE	IDENTIFIER
SK1 *MATa/MATalpha nuc1Δ::HygroB his4X::LEU2-(NgoMIV,+ori)-URA3/HIS4::LEU2-(BAMHI;ori)*	This study	YML5528
SK1 *MATa/MATalpha nuc1Δ::HygroB YEN1^{ON} his4X::LEU2-(NgoMIV,+ori)-URA3/HIS4::LEU2-(BAMHI;ori)*	This study	YML5530
SK1 *MATa/MATalpha nuc1Δ::HygroB ndt80Δ::NatMX4 his4X::LEU2-(NgoMIV,+ori)-URA3/HIS4::LEU2-(BAMHI;ori)*	This study	YML5772
SK1 *MATa/MATalpha nuc1Δ::HygroB ndt80Δ::NatMX4 YEN1^{ON} his4X::LEU2-(NgoMIV,+ori)-URA3/HIS4::LEU2-(BAMHI;ori)*	This study	YML5531
SK1 *MATa/MATalpha nuc1Δ::HygroB ndt80Δ::HIS3 mlh3Δ::KanMX6 his4X::LEU2-(NgoMIV,+ori)-URA3/HIS4::LEU2-(BAMHI;ori)*	This study	YML5877
SK1 *MATa/MATalpha nuc1Δ::HygroB ndt80Δ::HIS3 mlh3Δ::KanMX6 YEN1^{ON} his4X::LEU2-(NgoMIV,+ori)-URA3/HIS4::LEU2-(BAMHI;ori)*	This study	YML6379
SK1 *MATa/MATalpha CEN8/CEN8::tdTomato-LEU2 ARG4/ARG4:: GFP*-URA3 THR1/THR1::m-Cerulean-TRP1*	This study	YML3310
SK1 *MATa/MATalpha YEN1^{ON} CEN8/CEN8::tdTomato-LEU2 ARG4/ARG4:: GFP*-URA3 THR1/THR1::m-Cerulean-TRP1*	This study	YML3311
SK1 *MATa/MATalpha mlh1Δ::KanMX4 CEN8/CEN8::tdTomato-LEU2 ARG4/ARG4:: GFP*-URA3 THR1/THR1::m-Cerulean-TRP1*	This study	YML4534
SK1 *MATa/MATalpha mlh1Δ::KanMX4 YEN1^{ON} CEN8/CEN8::tdTomato-LEU2 ARG4/ARG4:: GFP*-URA3 THR1/THR1::m-Cerulean-TRP1*	This study	YML4535
SK1 *MATa/MATalpha mlh3Δ::KanMX4 CEN8/CEN8::tdTomato-LEU2 ARG4/ARG4:: GFP*-URA3 THR1/THR1::m-Cerulean-TRP1*	This study	YML3452
SK1 *MATa/MATalpha mlh3Δ::KanMX4 YEN1^{ON} CEN8/CEN8::tdTomato-LEU2 ARG4/ARG4:: GFP*-URA3 THR1/THR1::m-Cerulean-TRP1*	This study	YML3453
SK1 *MATa/MATalpha exo1Δ::KanMX4 CEN8/CEN8::tdTomato-LEU2 ARG4/ARG4:: GFP*-URA3 THR1/THR1::m-Cerulean-TRP1*	This study	YML4917
SK1 *MATa/MATalpha exo1Δ::KanMX4 YEN1^{ON} CEN8/CEN8::tdTomato-LEU2 ARG4/ARG4:: GFP*-URA3 THR1/THR1::m-Cerulean-TRP1*	This study	YML4918
SK1 *MATa/MATalpha mus81Δ::KanMX4 CEN8/CEN8::tdTomato-LEU2 ARG4/ARG4:: GFP*-URA3 THR1/THR1::m-Cerulean-TRP1*	This study	YML4321
SK1 *MATa/MATalpha mus81Δ::KanMX4 YEN1^{ON} CEN8/CEN8::tdTomato-LEU2 ARG4/ARG4:: GFP*-URA3 THR1/THR1::m-Cerulean-TRP1*	This study	YML4322
SK1 *MATa/MATalpha PDS1-myc18::KITRP1 ura3::tetOx224-URA3::tetR-GFP-HphMX4*	This study	YML4323
SK1 *MATa/MATalpha YEN1^{ON} PDS1-myc18::KITRP1 ura3::tetOx224-URA3::tetR-GFP-HphMX4*	This study	YML4324
SK1 *MATa/MATalpha mlh3Δ::KanMX4 PDS1-myc18::KITRP1 ura3::tetOx224-URA3::tetR-GFP-HphMX4*	This study	YML4325
SK1 *MATa/MATalpha mlh3Δ::KanMX4 YEN1^{ON} PDS1-myc18::KITRP1 ura3::tetOx224-URA3::tetR-GFP-HphMX4*	This study	YML4326
SK1 *MATa/MATalpha mus81Δ::KanMX4 PDS1-myc18::KITRP1 ura3::tetOx224-URA3::tetR-GFP-HphMX4*	This study	YML4327
SK1 *MATa/MATalpha mus81Δ::KanMX4 YEN1^{ON} PDS1-myc18::KITRP1 ura3::tetOx224-URA3::tetR-GFP-HphMX4*	This study	YML4328
SK1 *MATa/MATalpha mlh3Δ::KanMX4 sgs1::P$_{CLB2}$-HA3-SGS1::KanMX6 mus81Δ::HIS3 PDS1-myc18::KITRP1 ura3::tetOx224-URA3::tetR-GFP-HphMX4*	This study	YML4331
SK1 *MATa/MATalpha mlh3Δ::KanMX4 sgs1::P$_{CLB2}$-HA3-SGS1::KanMX6 mus81Δ::HIS3 YEN1^{ON} PDS1-myc18::KITRP1 ura3::tetOx224-URA3::tetR-GFP-HphMX4*	This study	YML4332
SK1 *MATa/MATalpha mlh1Δ::KanMX4*	This study	YML4865
SK1 *MATa/MATalpha mlh1Δ::KanMX4 yen1Δ::CNAT*	This study	YML4835

REAGENT or RESOURCE	SOURCE	IDENTIFIER
SK1 *MATa/MATalpha mlh1Δ::KanMX4 YEN1^{ON}*	This study	YML4862
SK1 *MATa/MATalpha mlh3Δ::KanMX4*	This study	YML3964
SK1 *MATa/MATalpha mlh3Δ::KanMX4 yen1Δ::NatMX*	This study	YML4006
SK1 *MATa/MATalpha mlh3Δ::KanMX4 YEN1^{ON}*	This study	YML4007
SK1 *MATa/MATalpha exo1Δ::KanMX4*	This study	YML4827
SK1 *MATa/MATalpha exo1Δ::KanMX4 yen1Δ::CNAT*	This study	YML4828
SK1 *MATa/MATalpha exo1Δ::KanMX4 YEN1^{ON}*	This study	YML4856
SK1 *MATa/MATalpha sgs1Δ::KanMX4*	This study	YML4897
SK1 *MATa/MATalpha sgs1Δ::KanMX4 yen1Δ::CNAT*	This study	YML4898
SK1 *MATa/MATalpha sgs1Δ::KanMX4 YEN1^{ON}*	This study	YML4899
SK1 *MATa/MATalpha mus81Δ::HIS3*	This study	YML2782
SK1 *MATa/MATalpha mus81Δ::HIS3 yen1Δ::TRP1*	This study	YML2783
SK1 *MATa/MATalpha mus81Δ::HIS3 YEN1^{ON}*	This study	YML2784
SK1 *MATa/MATalpha mus81Δ::HIS3 mlh3Δ::KanMX4*	This study	YML4005
SK1 *MATa/MATalpha mus81Δ::HIS3 mlh3Δ::KanMX4 yen1Δ::CNAT*	This study	YML3965
SK1 *MATa/MATalpha mus81Δ::HIS3 mlh3Δ::KanMX4 YEN1^{ON}*	This study	YML3966
SK1 *MATa/MATalpha mus81Δ::HIS3 mlh3Δ::KanMX4 sgs1::* P_{CLB2}*-HA3-SGS1::KanMX6*	This study	YML3969
SK1 *MATa/MATalpha mus81Δ::HIS3 mlh3Δ::KanMX4 sgs1::* P_{CLB2}*-HA3-SGS1::KanMX6 yen1Δ::TRP1*	This study	YML3970
SK1 *MATa/MATalpha mus81Δ::HIS3 mlh3Δ::KanMX4 sgs1::* P_{CLB2}*-HA3-SGS1::KanMX6 YEN1^{ON}*	This study	YML3971
SK1 *MATa/MATalpha srs2Δ::KanMX4*	This study	YML4701
SK1 *MATa/MATalpha srs2Δ::KanMX4 yen1Δ::CNAT*	This study	YML4675
SK1 *MATa/MATalpha srs2Δ::KanMX4 YEN1^{ON}*	This study	YML4702
SK1 *MATa/MATalpha*	This study	YML2776
SK1 *MATa/MATalpha YEN1^{ON}*	This study	YML2778
SK1 *MATa/MATalpha spo11Δ::KITRP1 mam1Δ::HIS3*	This study	YML3974
SK1 *MATa/MATalpha spo11Δ::KITRP1 mam1Δ::HIS3 YEN1^{ON}*	This study	YML3975
SK1 *MATa/MATalpha msh4Δ::KanMX4 CEN8/CEN8::tdTomato-LEU2 ARG4/ARG4:: GFP*-URA3 THR1/THR1::m-Cerulean-TRP1*	This study	YML3588
SK1 *MATa/MATalpha msh4Δ::KanMX4 YEN1^{ON} CEN8/CEN8::tdTomato-LEU2 ARG4/ARG4:: GFP*-URA3 THR1/THR1::m-Cerulean-TRP1*	This study	YML3589
SK1 *MATa/MATalpha nuc1Δ::HygroB ndt80Δ::NatMX4 ura3::*P_{GPD}*-GAL4-ER-URA3* P_{GAL1}*-YEN1^{WT}-FTH::TRP1 his4X::LEU2-(NgoMIV,+ori)-URA3/HIS4::LEU2-(BAMHI;ori)*	This study	YML4224
SK1 *MATa/MATalpha nuc1Δ::HygroB ndt80Δ::NatMX4 ura3::* P_{GPD}*-GAL4-ER-URA3* P_{GAL1}*-YEN1^{ON}-FTH::TRP1 his4X::LEU2-(NgoMIV,+ori)-URA3/HIS4::LEU2-(BAMHI;ori)*	This study	YML4223
SK1 *MATa/MATalpha nuc1Δ::HygroB ndt80Δ::NatMX4 ura3::* P_{GPD}*-GAL4-ER-URA3* P_{GAL1}*-YEN1$^{ON\text{-}ND}$-FTH::TRP1 his4X::LEU2-(NgoMIV,+ori)-URA3/HIS4::LEU2-(BAMHI;ori)*	This study	YML6376

REAGENT or RESOURCE	SOURCE	IDENTIFIER
SK1 *MATa/MATalpha ndt80Δ::NatMX4 ura3::* P_{GPD}*-GAL4-ER-URA3* P_{GAL}*-YEN1^{ON}-FTH::TRP1 mlh1Δ::KanMX4 his4X::LEU2-(NgoMIV,+ori)-URA3/HIS4::LEU2-(BAMHI;ori)*	This study	YML6613
SK1 *MATa/MATalpha nuc1Δ::HygroB ndt80Δ::NatMX4 ura3::* P_{GPD}*-GAL4-ER-URA3* P_{GAL}*-YEN1^{ON}-FTH::TRP1 mlh3Δ::KanMX4 his4X::LEU2-(NgoMIV,+ori)-URA3/HIS4::LEU2-(BAMHI;ori)*	This study	YML6530
SK1 *MATa/MATalpha nuc1Δ::HygroB ndt80Δ::NatMX4 ura3::* P_{GPD}*-GAL4-ER-URA3* P_{GAL}*-YEN1^{ON}-FTH::TRP1 Mlh3-ND-myc9::KanMX4 his4X::LEU2-(NgoMIV,+ori)-URA3/HIS4::LEU2-(BAMHI;ori)*	This study	YML6653
SK1 *MATa/MATalpha ndt80Δ::NatMX4 ura3/ura3::*P_{GPD}*-GAL4-ER-URA3 leu2/leu2::*P_{GAL}*-NDT80-LEU2 KanMX4::*P_{CUP}*-YEN1^{ON}-myc9::KITRP1 CEN8/CEN8::tdTomato-LEU2 ARG4/ARG4:: GFP*-URA3 THR1/THR1::m-Cerulean-TRP1*	This study	YML5414
SK1 *MATa/MATalpha ndt80Δ::NatMX4 ura3/ura3::*P_{GPD}*-GAL4-ER-URA3 leu2/leu2::*P_{GAL}*-NDT80-LEU2 CEN8/CEN8::tdTomato-LEU2 ARG4/ARG4:: GFP*-URA3 THR1/THR1::m-Cerulean-TRP1*	This study	YML5486
S. cerevisiae S96 *MATa ho lys5*	Fung lab	S96
S. cerevisiae YJM789 *MATalpha ho::hisG lys2 cyh*	Fung lab	YJM789
S96/YJM789	This study	YML3684
S96/YJM789 *YEN1^{ON}*	This study	YML3685
S96/YJM789 *mlh3Δ::KanMX6*	This study	Fung lab
S96/YJM789 *msh4::KanMX6*	This study	Fung lab
S96/YJM789 *YEN1^{ON} mlh3Δ::KanMX6*	This study	YML4344
S96/YJM789 *YEN1^{ON} msh4Δ::KanMX6*	This study	YML4214
Software and Algorithms		
ReCombine	Anderson et al. 2011 (Anderson et al., 2011)	
Stahl lab online tools	(Stahl and Lande, 1995)	http://elizabethhousworth.com/StahlLabOnlineTo